CubeSat Power System Implementing a Zero Voltage Switching Resonant Buck Converter Design with Low Electronic & Radio Frequency Noise

A Thesis

Presented in Partial Fulfillment of the Requirements for the

Degree of Master of Science

with a

Major in Electrical Engineering

in the

College of Graduate Studies

University of Idaho

by

Christine Page

Approved by:

Major Professor: Herbert Hess, Ph.D.

Committee Members: Kerri Cahoy, Ph.D.; Brian K. Johnson, Ph.D.

Department Administrator: Joseph Law, Ph.D.

May 2022

Abstract

This thesis presents how radio frequency electromagnetic noise from power supplies can be a limiting factor in how well scientific instruments on CubeSats can perform. Instruments such as microwave radiometers, wide-band software defined radios, or precipitation instruments are all affected by electronic and radio frequency (RF) noise. Current hybrid DC/DC converter technologies can also be prone to failure and anomalies during flight. A solution to this problem is to create a DC/DC power converter with a low-noise circuit design. This thesis presents a solution for a CubeSat power supply to become more effective and efficient by reducing the noise coupled through power supply switching so that the power converter does not affect the CubeSat instruments. A fully integrated solution has reduced noise on the output of the soft-switching resonant buck converter device. This design includes a fixed frequency and variable capacitor for its control scheme and has been validated by a build-and-test method.

Acknowledgements

I don’t have enough words to express my gratitude for the people who have helped and supported me to get this far in my life.

Dr. Herbert Hess and Dr. Brian K. Johnson took a chance and gave me a research position during my freshman year of undergrad when I had zero knowledge of electrical engineering. They both mentored me through the research process, providing me with endless opportunities for the past six years. There were no restrictions to what they allowed me to do, and I would not be where the person I am now without their guidance and support.

Dr. Kerri Cahoy provided me with amazing opportunities that have changed the trajectory of my life in the best way. I am so grateful for her kindness and generosity. Giving me a chance to be mentored by her while pursuing the work presented in this thesis has been such an honor.

I salute and cherish the friends who have supported me throughout the entire journey of the thesis process. Getting to this point wasn’t easy, but them being on call for hours while I worked on my horrible soldering skills kept me sane.

My parents Edward and Song Page are my biggest cheerleaders as well as my biggest support throughout my entire life. They have instilled in me the importance of hard work and have always wished for my happiness in every aspect of my life. There have been endless calls and home-visits throughout my entire time at University of Idaho, and this thesis would not exist if not for them.

Dedication

This thesis is dedicated to my parents who always support me and my dreams.

Table of Contents

List of Tables

List of Figures

List of Abbreviations

CubeSat	Cube Satellite
C_r	Resonant Capacitor
DC	Direct Current
DC/DC	Direct Current to Direct Current
EMI	Electromagnetic Interference
EPS	Electrical Power System
ESL	Equivalent Series Inductance
ESR	Equivalent Series Resistance
FFO	Fixed Frequency Oscillator
JPL	Jet Propulsion Laboratory
MOSFET	Metal Oxide Semiconductor Field Effect Transistor
NASA	National Aeronautics and Space Administration
PCB	Printed Circuit Board
PDM	Pulse Density Modulation
PFD	Phase Frequency Detector
PLL	Phase Lock Loop
P-N	Positive-Negative
PWM	Pulse Width Modulation
RF	Radio Frequency
RFI	Radio Frequency Interference
SmallSat	Small Satellite
SNR	Signal-to-Noise Ratio
VCO	Voltage Controlled Oscillator
ZVS	Zero Voltage Switching

1.0 INTRODUCTION

CubeSats are small satellites with fewer size, weight, and power resources and deployment costs. CubeSats allow for testing new payload technologies, such as testing novel weather instruments. CubeSats also can be deployed in large numbers to different orbits to improve temporal and spatial coverage. CubeSat missions need power supplies that are both efficient and low noise.

In NASA's Strategic Plan for the years 2018-2021, it states, "A balanced science program proactively identifies potential technologies required to meet future mission requirements, conduct trade studies, assess development risks, and invests in new technologies well in advance of mission implementation. NASA is also expanding the use of lower-cost CubeSats and SmallSats to accomplish our science goals." [1] NASA has an interest in the development of CubeSats since they are cost effective ways of testing new and improved technologies. They are less expensive to build as well as launch. To be able to optimize the performance of CubeSats, we seek to better support payload instrument sensitivity. The 2020 NASA Technology Taxonomy mentions "Remote sensing instruments and sensors include components, sensors, and instruments sensitive to electromagnetic radiation; particles (charged, neutral, dust); electromagnetic fields, both direct current (DC) and alternating current (AC)..." [2]

Current hybrid power converter technologies can generate RF noise and other electromagnetic interference (EMI). DC/DC converters can also have anomalies and failures. For example, the GRACE mission had reported converter failure due to high temperatures, which caused a reduction in switching frequency [3][4]. Other missions involving the International Space Station and Hubble Space Telescope have also reported

converters failing during flight [3]. This research project will develop a more effective and efficient CubeSat power supply by reducing the noise coupled through power supply switching. This will help pave the way for CubeSats to support a wider range of missions.

1.1 Effects of Noise

Conducted noise from power supplies can be a limiting factor in how well scientific instruments on CubeSats can perform. Instruments such as microwave radiometers which are on TROPICS, TEMPEST-D, and IceCube, or wide-band software defined radios used on AERO-VISTA for Earth auroral hiss observations, or precipitation instruments used on RainCube are all affected by electronic and radio frequency (RF) noise.

An example of the difference between noise and a desired signal is shown in Figure 1-1.

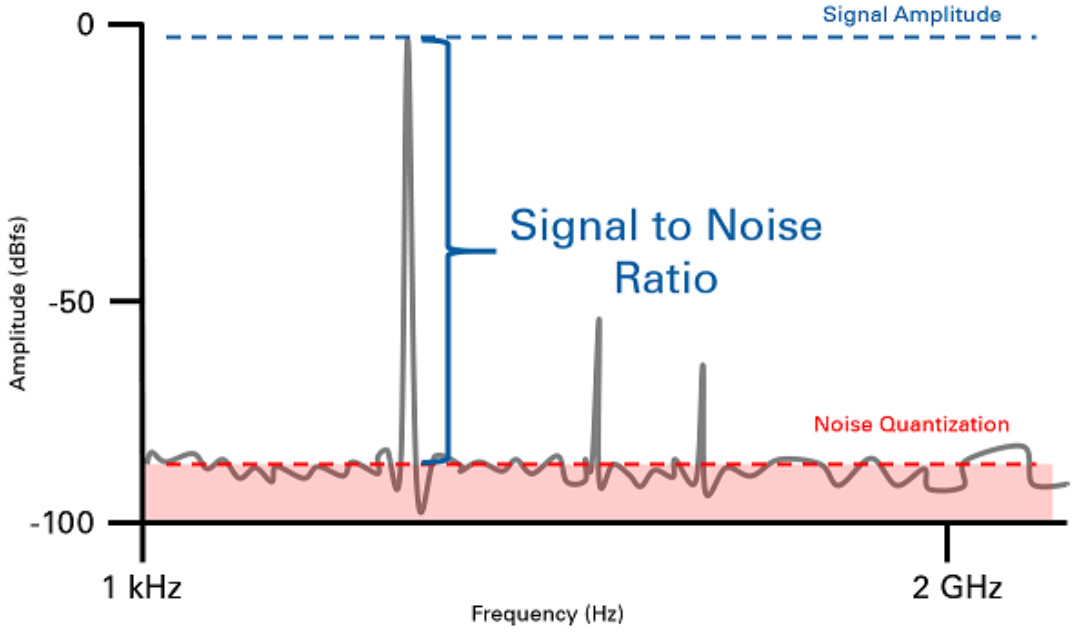

Figure 1-1. Noise vs. Desired Signal [5]

The signal to noise ratio (SNR) is the ratio between the desired signal and undesired signal also known as noise. Noise can come into the measurement from the environment, from the sensors or instruments being used, or from the transmission between the signal device to the recording display. Another way noise can enter the recorded measurements is by conduction from the power supplies supplying power to the CubeSat and its instruments, this is known as electrical noise.

For an example of how noise can affect a radio-frequency instrument, consider Figure 1-2 [6], which shows sample images collected with the Jet Propulsion Laboratory's (JPL's) AIRSAR P-band radar system.

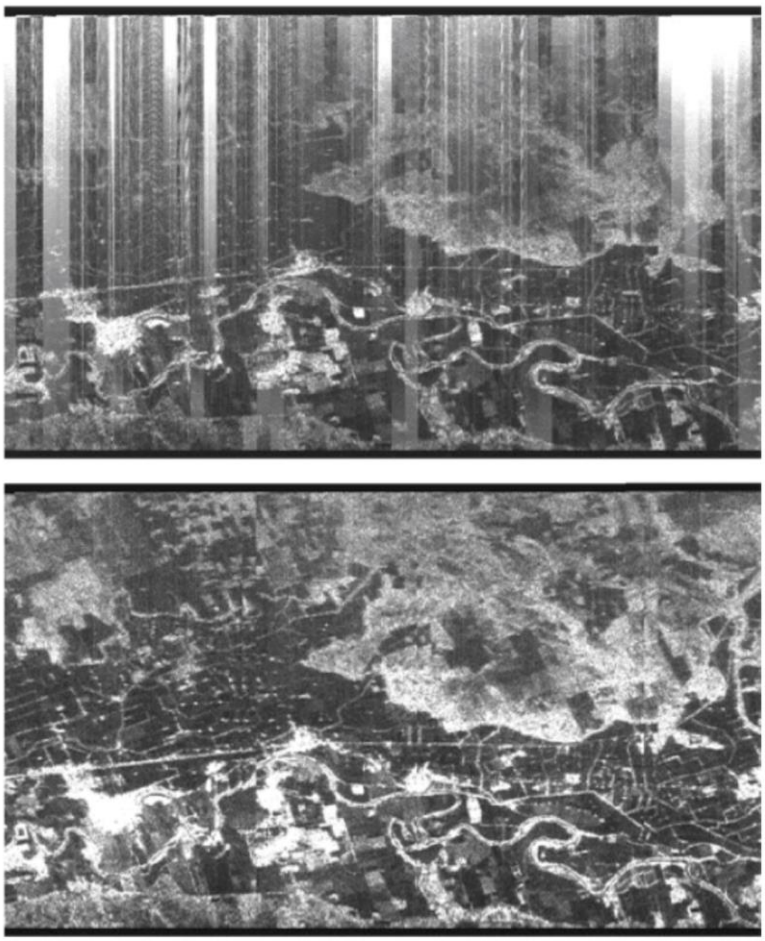

Figure 1-2. Sample images collected with the Jet Propulsion Laboratory's (JPL's) AIRSAR P-band radar system. The top image shows RFI. [6]

The first image shows how the radio frequency (RF) interference noise corrupts the data, causing the image to become disjointed and whited-out. The second image was taken after a noise mitigation technique was applied to the AIRSAR P-band radar system. [6] Figure 1-2 shows how important decreasing the amount of noise coupled to instruments is, as RF noise can significantly affect performance.

1.2 Power Supply Noise

A noise evaluation study was done on a basic buck converter with a 200 kHz switching frequency. RF probes and a spectrum analyzer (EN55011 [7]) were used to make measurements. The results are shown in Figure 1-3 [8] where the buck converter located 1.0 m above the ground plane, on wood table, and 3.0 m from the receiving antenna (horizontal polarization).

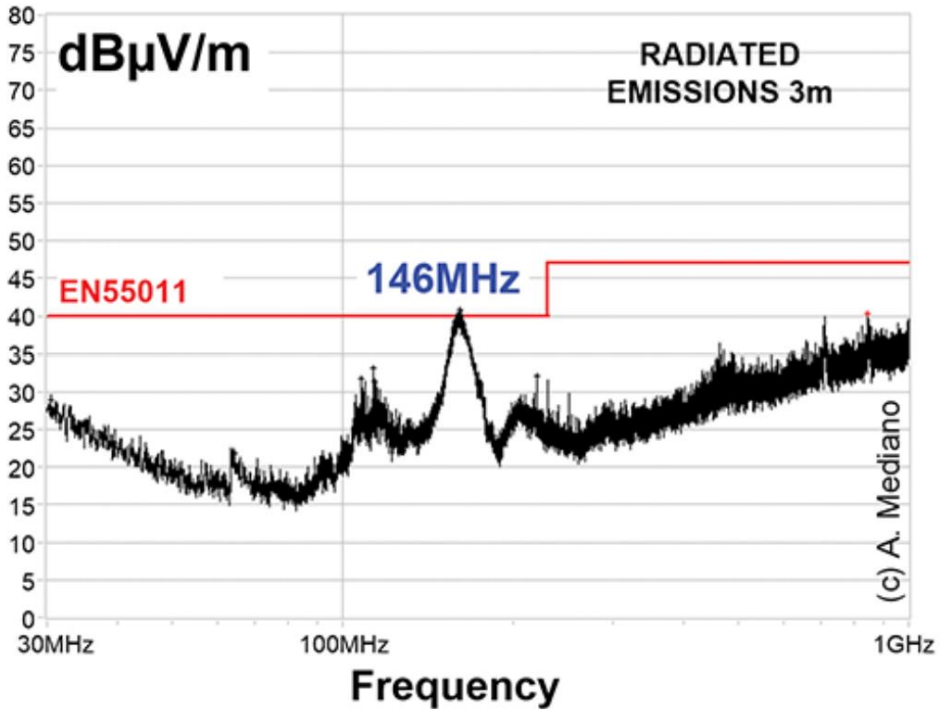

Figure 1-3. Test study of noise of a buck converter measured by near field probes [8]

Noise peaked at about 150 MHz at a value of around 40 dB µV/m due to the output of the buck converter. This measurement is used as the baseline goal for the buck converter design since it encompasses similar specifications and uses an exact noise measurement. This also shows why CubeSats need to address the noise issue of the power converter in addition to integrating noise mitigation techniques for sensor instruments and other parts of the satellite.

CubeSats currently use filtering noise techniques to address this RF electromagnetic interference issue. Figure 1-4 [9] shows an example of a buck converter voltage output after an L-C filter is added to dampen the switching output noise.

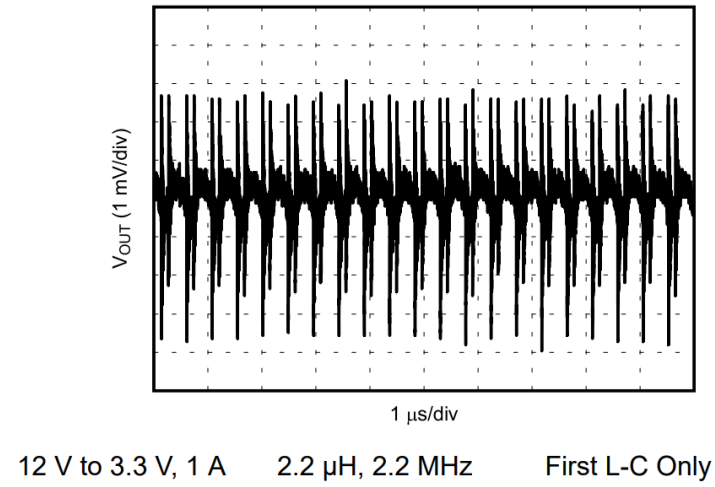

Figure 1-4. Vout Ripple after a one stage L-C filter [9]

Figure 1-4 clearly shows that the output is still being affected by the hard-switching of the buck converter device even with the L-C filter. Without a resistive load to dampen the effect, it becomes clearer from Figure 1-4 that hard-switching of the DC/DC causes high RF noise and output voltage ripple, even with a L-C filter added to decrease the noise.

Figure 1-4 also shows that the noise output caused by the ringing response of the circuit or power supply due to hard-switching has not yet been resolved. A different approach is needed to mitigate the problem.

Power converters generally use a pulse width modulation (PWM) scheme that is modified by varying duty cycle which will determine how long the device stays on or off. Some scheme also vary the switching frequency as another a way to control the overall voltage output of the converter. This is a beneficial way to power various loads that CubeSats are required to have onboard. However, varying the switching frequency varies how the voltage pulses from the regulator are coupled to the rest of the circuit, causing increased voltage ripple and output converter noise. Therefore, a more optimized DC/DC power converter is needed where the switching frequency is not varied to change the voltage output without increasing noise output.

1.3 Thesis Objectives

The goal of this thesis is to present and prove a design of a compact power converter with reduced RF noise to reduce the electrical power system (EPS)'s effects on a CubeSat's onboard instruments. A fully integrated solution has reduced noise on the output of the soft-switching resonant buck converter device. This design includes a fixed frequency and variable capacitor for its control scheme.

1.4 Thesis Organization

The thesis is organized into 6 chapters. Chapter 2 will discuss the basic DC/DC buck converter topology and current noise damping techniques while also reviewing the current issues with hard-switching schemes. Chapter 3 will provide an overview of resonant converters and present work on a new resonant converter design and control

scheme. Chapter 4 will present my results that prove noise reduction with my resonant converter design and control scheme. Chapter 5 will draw conclusions to the thesis. Finally, suggestions for improving the resonant converter and control scheme will be summarized and presented in Chapter 6.

2.0 DC/DC POWER CONVERTERS

When regulating power in CubeSats, DC/DC power converters switch semiconductor devices at high frequency in the circuit, effectively keeping the average voltage at the output constant by varying the current [10]. Although this method is power-efficient, it generates high amounts of noise due to sharp voltage and current transitions from switching. This work focuses on the development of a DC/DC power converter design that will be applicable for all power converters in the electrical power system (EPS) for a CubeSat. An example of a typical CubeSat EPS layout and requirement output voltages from power converters is shown in Figure 2-1 [11].

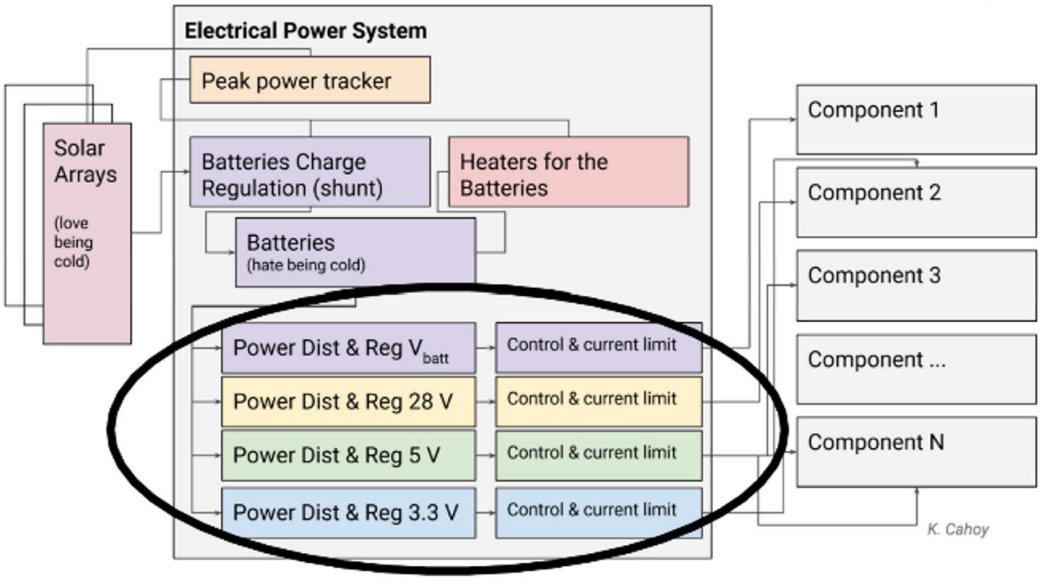

Figure 2-1. Block diagram of a typical CubeSat power system [11]

The typical electrical characteristics for DC/DC power converters in the EPS of a CubeSat are shown in Table 2-1 [12].

Table 2-1. Electrical Characteristics of a DC/DC Power Converter [12]

Description	Conditions	Min	Typical	Max	Unit
Input Voltage		7.4	--	30	V
Output Voltage	5V Bus	4.95	5	5.05	V
	3.3V Bus	3.26	3.3	3.33	V
Switching Frequency	For 5V & 3.3V	100	150	200	kHz

The noise from the power converter couples into the scientific measurements being made. A solution to this problem is to create a DC/DC power converter with a low-noise circuit design. This proposed low-noise power converter uses resonant frequency, not voltage level, to communicate control information, giving the power converter an inherent immunity to high noise levels, including those caused by switching. An example of a simple conventional buck converter schematic as presently used is shown in Figure 2-2 [10].

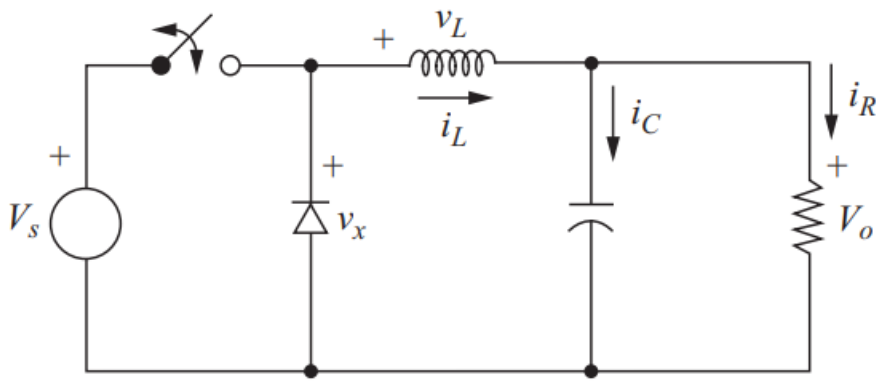

Figure 2-2. DC/DC Buck Converter Schematic [10]

Although the DC/DC buck power converter is noisy, it is still widely used due to its compact and simplistic design, and it is also cheap to manufacture or buy. The goal of the buck converter is to step-down the voltage from the input source to the output facing a load.

2.1 Buck Converter Design w/ Capacitor Filters

Figure 2-3 shows a standard buck converter design with capacitor filters implemented as a noise mitigation technique. The capacitor C2 is used to mitigate the noise coming from the input source VIN and the capacitor C3 is used to mitigate the noise caused by the hard-switching PWM of MOSFET M1.

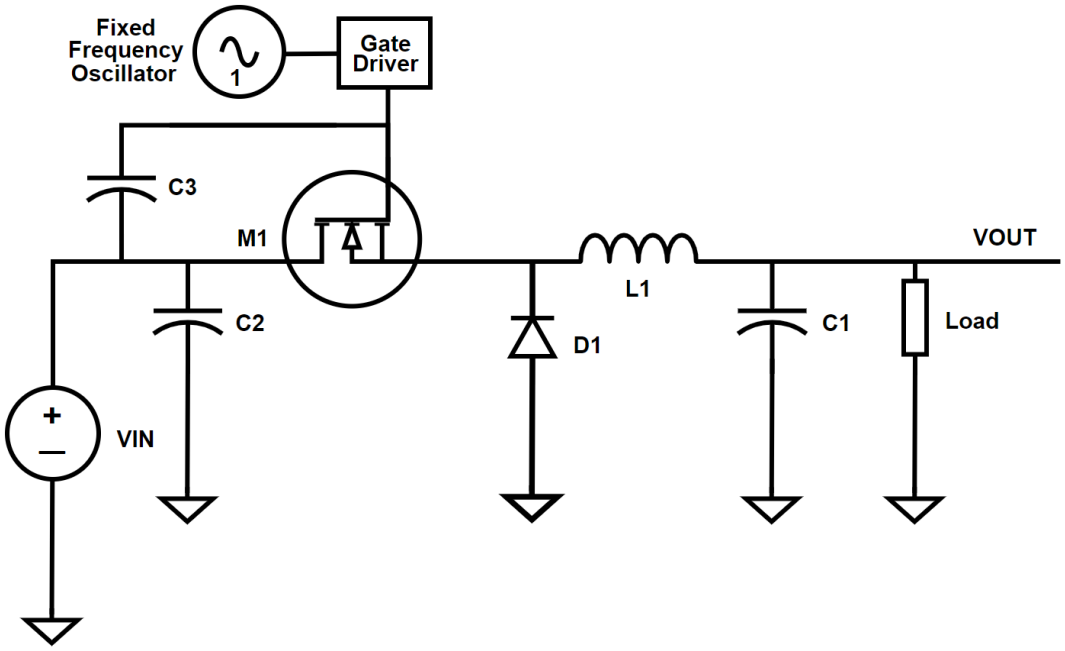

Figure 2-3. Buck Converter w/ Capacitor Filters [Christine Page]

Figure 2-4 shows the buck converter PCB for the circuit of Figure 2-3 built for evaluating filter performance based on the design in Figure 2-3.

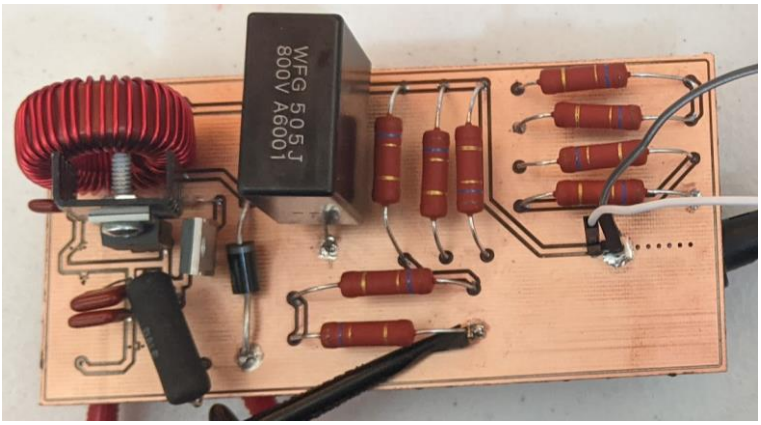

Figure 2-4. Buck Converter PCB w/ Capacitor Filters [Christine Page]

A metallized polypropylene film capacitor was chosen for the capacitor C1 because it is mostly used for automotive applications, where it performs well in switching DC/DC converters, high frequency circuits, and large current circuits to decrease output RF noise and output voltage ripple.

The capacitor value was determined by using Equation (2.1).

$$C = \frac{1-D}{8*L*(\Delta V_o/V_o)*f^2} \tag{2.1}$$

where f is the frequency, D is the duty cycle, L is the inductance value, V_o is the converter output voltage, and ΔV_o is the desired limit peak-to-peak ripple output voltage.

The importance of selecting a capacitor that can handle a switching application has to do with the non-ideal characteristics of the capacitor as shown in Figure 2-5, where ESR is the Equivalent Series Resistance and ESL is the Equivalent Series Inductance.

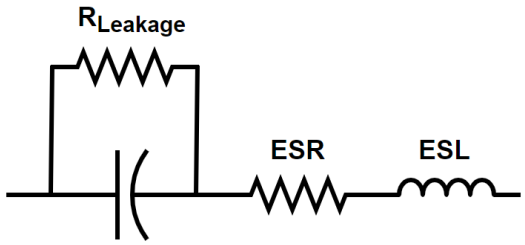

Figure 2-5. Non-Ideal Capacitor [Christine Page]

A high ESR value will cause the capacitor to dissipate heat in high current applications. A low ESR values helps with noise filtering which overall helps the performance of a circuit such as a buck converter.

Equation (2.2) shows how to calculate the ESR.

$$ESR = \frac{1}{2*\pi*f*Q} \tag{2.2}$$

where f is the main power converter switching frequency and Q is the quality factor from the capacitor's datasheet.

A high ESL value will couple high amounts of noise into other parts of the circuit. It could also cause the capacitor to malfunction in some applications. A voltage ringing will be generated, causing the circuit to perform undesirably and inefficiently.

Equation (2.3) shows how to calculate the ESL.

$$ESL = \frac{1}{4*\pi^2*f^2*C} \tag{2.3}$$

where f is the main power converter switching frequency and C the capacitance value.

A toroidal choke inductor was chosen for L1 because it acts like a low pass filter for high frequency switching PWM signals. At higher frequencies, the internal capacitances of the inductor, such as interwinding capacitances, become significant influences on its operation.

The inductor value is calculated using Equation (2.4).

$$L = \frac{(1-D)*R}{2*f} \quad (2.4)$$

where f is the frequency, D the duty cycle, and R is the equivalent load resistance.

The fabricated PCB was made as small as possible (5cm by 8cm) to be able to reduce the amount of cross coupling of noise between current paths by having short trace lengths. The traces were made as thick as possible (50 mil) to be able to handle the high amount of current being outputted by the converter.

2.2 Noise Test Results for Buck Converter w/ Capacitor Filters

Figure 2-6 shows the voltage at the MOSFET's output in yellow and the buck converter output voltage in green.

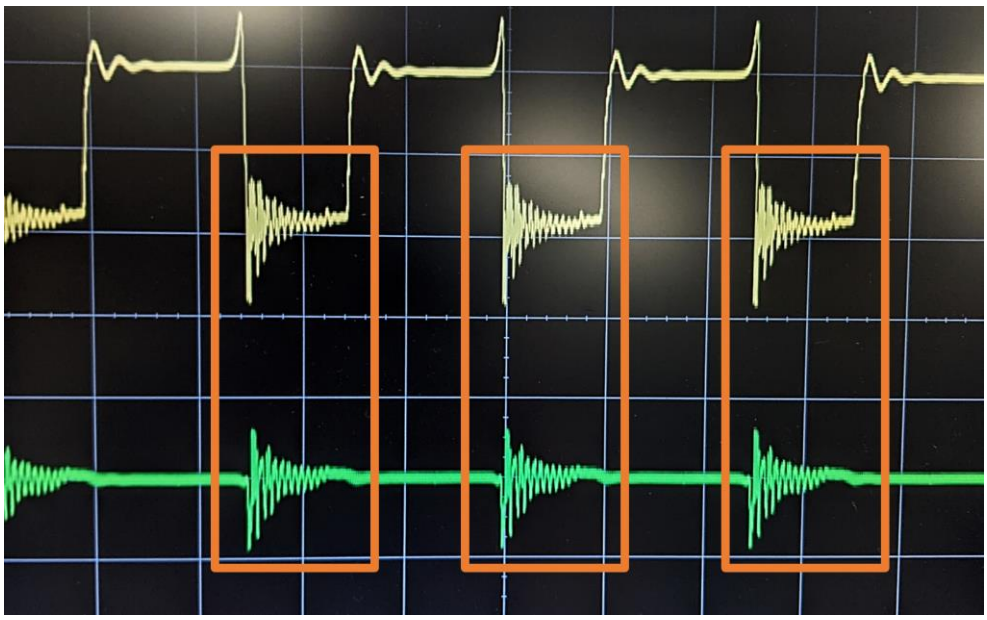

Figure 2-6. MOSFET Voltage Output vs. Buck Converter Voltage Output

Figure 2-6 shows the noise due to the hard-switching PWM highlighted in the orange boxes. Each time the MOSFET switches off (yellow), it causes oscillations on the output voltage (green). This is due to the conducted noise.

2.3 Resonant DC/DC Converter

Two classes of schemes most commonly used to modulate a DC/DC converter output: (1) Pulse width modulation (PWM) schemes characterized by hard switching, and (2) soft switching schemes used in resonant or quasi-resonant converters.

PWM regulates power by varying the duty cycle to control current flow and output voltage. PWM schemes have hard switching on both turn-on and turn-off, which causes high switching power loss but has low conduction loss. Soft switching is when a resonant power converter operating at a frequency lower than resonance yields a zero-voltage turn-off with substantially less switching noise. The resonance behavior causes the voltage across the switching device to be zero at the time the turn off command it send to the device. Since switching losses are the product of voltage and current during the turn off period, this zero-voltage turn-off brings the turn-off losses to zero. This zero-voltage switching (ZVS) one possible soft switching scheme in the family of resonant converter schemes. The focus is on voltage turn-off on the MOSFET due to it being the source of RF emissions on the buck converter. The conduction losses are similar to or slightly higher than comparable PWM-based power converters. The drawbacks of resonant converters are that the power devices will carry higher peak current values as well as increase the complexity of the circuit due to needing a control scheme to operate.

A comparison between the hard-switching PWM scheme and the ZVS switching scheme is shown in Figure 2-7 (a) and Figure 2-7 (b), respectively, as waveforms [13].

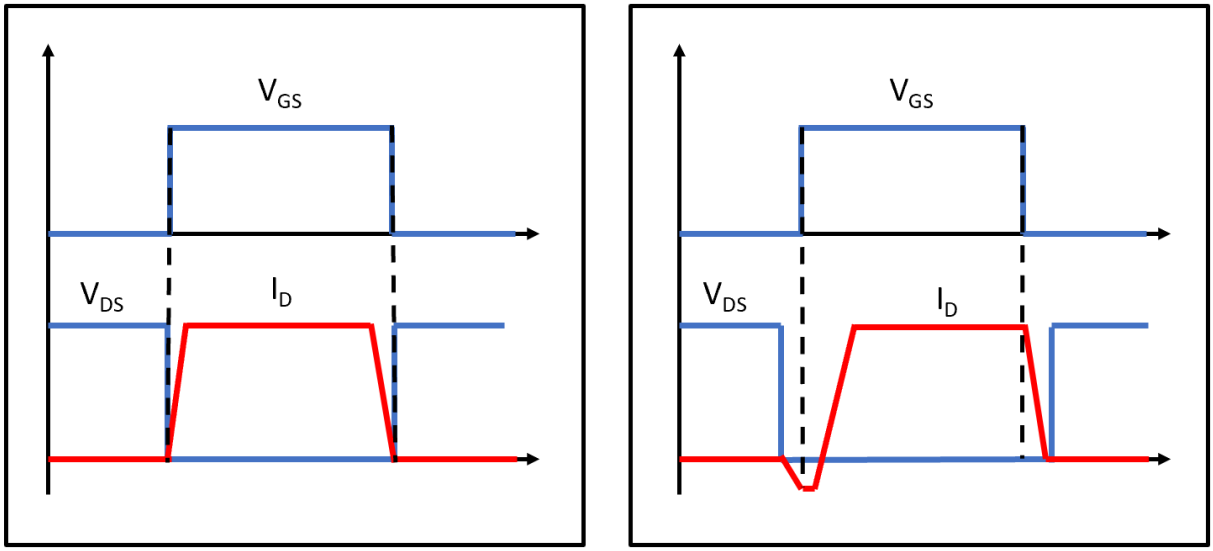

(a) Hard-Switching **(b) ZVS Switching**

Figure 2-7: Hard Switching vs. ZVS Switching [13, modified by Christine Page]

Combining these two switching schemes will be beneficial in creating a type of power converter that has better conduction efficiency and less switching noise. Creating a quasi-resonant power converter that can incorporate both PWM and zero voltage switching will reduce the noise of the overall system.

A quasi-resonant converter works by using a resonant switching element consisting of a MOSFET that generates a resonant pulse that is then filtered by the output inductor and capacitor. An example of a quasi-resonant buck converter is shown in Figure 2-8.

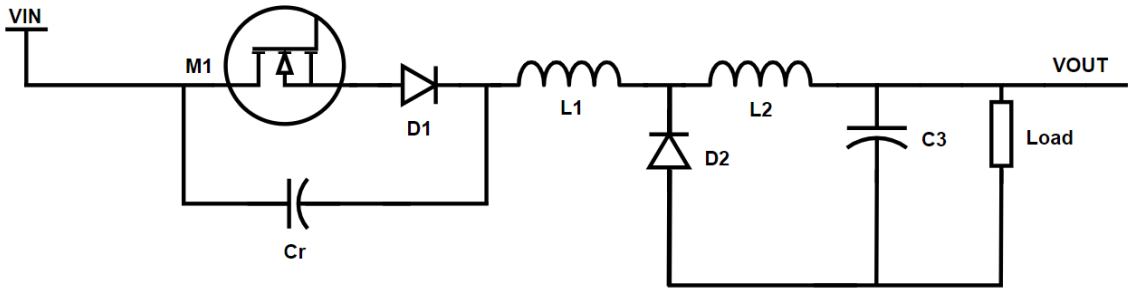

Figure 2-8: Quasi-resonant buck converter with ZVS switch [Christine Page]

2.4 Chapter Summary

CubeSats use DC/DC power converters to regulate power. A basic buck converter using hard-switching PWM schemes produces radiates noise on the output of the converter. The radiated noise from the buck converter output affects a CubeSat's instruments. A quasi-resonant power converter operating at a frequency lower than resonance yields a soft-switching scheme with substantially less switching noise.

3.0 RESONANT BUCK CONVERTER

The proposed control scheme is a phase-lock loop (PLL) control scheme designed to reduce noise and improve signal integrity. The power converter switching control uses the phase-locking technique to perform the comparison function in a feedback control system. Two voltage-controlled oscillators are implemented into the design. One of the oscillators operates at a reference frequency. The other oscillator operates at a frequency that is a function of output voltage feedback. A phase frequency detector (PFD) compares the two frequencies to determine the error signal, also a frequency, as shown in Figure 3-1 [14].

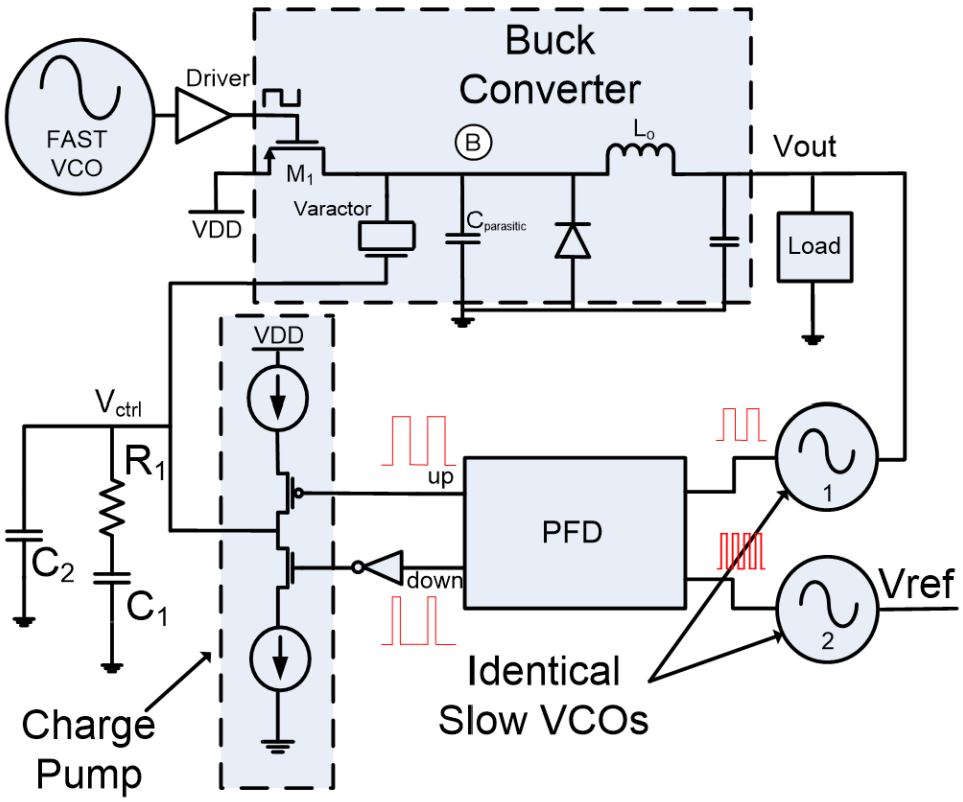

Figure 3-1: Phase-locking control scheme to reduce the output RFI [14]

In normal operation, when the controller generates an output voltage slightly lower than required, the PFD compares the rising edges of the two oscillator waveforms and produces up-signals that have a larger pulse width to pump more current from the dependent current sources in the charge pump into the resonant filter. The filter contains a varactor or a variable capacitance. This increased input to the filter will change the filter's resonant frequency and increase the filter's output voltage and command a greater duty cycle, correcting the error. The operation of this control loop is quite typical of this type of resonant converter controls: varying a PWM oscillator frequency relative to a resonant filter in response to feedback. Instead of a fixed component resonant filter to produce an error signal, the resonant controls in the design from [14] operate at a fixed switching frequency and the resonant filter varies its resonant frequency in response to an error signal. Because the information in these signals is contained in the frequency, the control is noise resistant [15].

The design is compact and inexpensive. The dimensions of the final PCB board is described in Section 3.3. The components used for the design are inexpensive commercial components. The high frequency design offers small-sized passives and a higher quality factor (Q) inductor. The design uses a tunable resonant frequency and a tunable Q factor by using variable capacitance values, which creates a variable resonance in combination with a fixed switching frequency to regulate the output voltage. This is the reverse of the typical resonant power converter controls that have a fixed resonant circuit and a variable frequency oscillator.

3.1 Resonant Converter Design & Simulation Results

Figure 3-2 shows a diagram of the implemented ZVS resonant buck converter with variable capacitor design as modeled in Simulink.

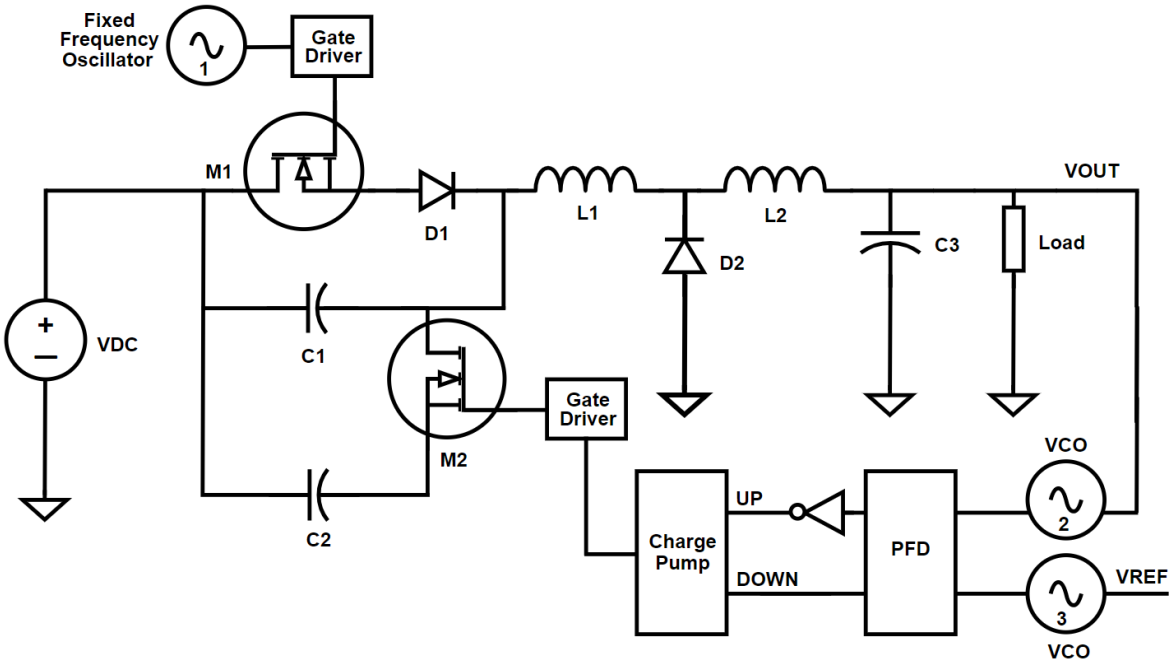

Figure 3-2. ZVS resonant buck converter with variable capacitor modeled in Simulink [Christine Page]

The variable capacitor is modeled as two capacitors in parallel, as shown in Figure 3-2. C1 is the main resonant capacitor. C2 is the capacitor that is connected in series with a MOSFET M2 that is switched by the resonant controls to vary the effective capacitance value of the circuit. Thus the effective capacitance of the resonance circuit is varied as a function of the applied switching frequency and duty cycle. For design purposes, C2 is about 1% of the value of C1.

Table 3-1 shows the values of the components referenced in Figure 3-2.

Table 3-1. Table of Values for Resonant Converter Components

Description	Value
Switching Frequency	200 kHz
Resonant Frequency	210 kHz
VDC	12 V
VOUT	5 V
VREF	5 V, 200 kHz
VCO 1	10 V, 200 kHz
VCO 2	VOUT
VCO 3	VREF
C1	130 nF
C2	1 nF
C3	10 uF
L1	4.5 uH
L2	2.5 uH
Load	1.6 ohms

The resonant frequency f_0 is determined using (3.1).

$$f_0 = \frac{1}{2*\pi*\sqrt{Cr*L1}} \tag{3.1}$$

Where Cr is the effective capacitance, as will be explained below. The switching frequency of M1 is 200 kHz. To be able to reduce the effect of switching noise on the output, the resonant frequency of the resonant converter must be on the edge of the resonant curve of 200 kHz. A resonant frequency above 200 kHz but less than 210 kHz will accomplish this. Figure 3-3 shows the variable effective resonant capacitor on the resonant curve.

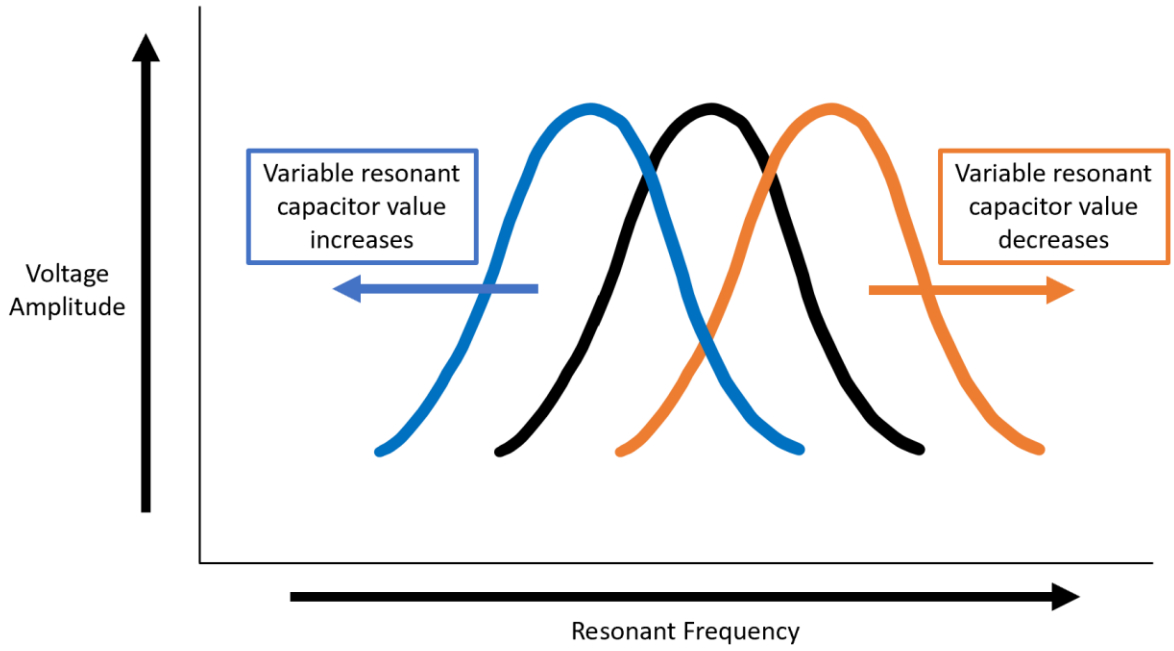

Figure 3-3. Resonant curve graph [Christine Page]

The resonant curve is used for regulating the voltage on the output of the resonant converter. To do so, the converter does not operate at the peak of the resonant curve. The resonant converter design shown in Figure 3-2 operates on the lower frequency side of the resonant curve. As the effective resonant capacitor, Cr, increases or decreases, the location of the resonance curve shifts left or right respectively. When moving the resonant curve location to the left, the intersection at the fixed switching frequency rises to a higher voltage.

The main switching frequency of the converter is fixed at 200kHz. The total resonant capacitance Cr was determined by combining capacitors C1 and C2 effectively connected in parallel with each other. A small voltage change on the output was desired, so the value of C2 was selected as 1% of the value of C1. These two design calculations are shown in Equations (3.2) and (3.3), respectively, where Equation (3.2) is the effective capacitance when M2 is in the on state.

$$Cr = C1 + C2 \tag{3.2}$$

$$C2 = C1 * 1\% \quad (3.3)$$

To have a larger variation of the output voltage, Eq. (3.3) could set C2 at 50% of C1.

Figure 3-4 shows the simulation results using the measurements stated in Table 3-1 for the ZVS resonant buck converter with C2 set at 1% of C1.

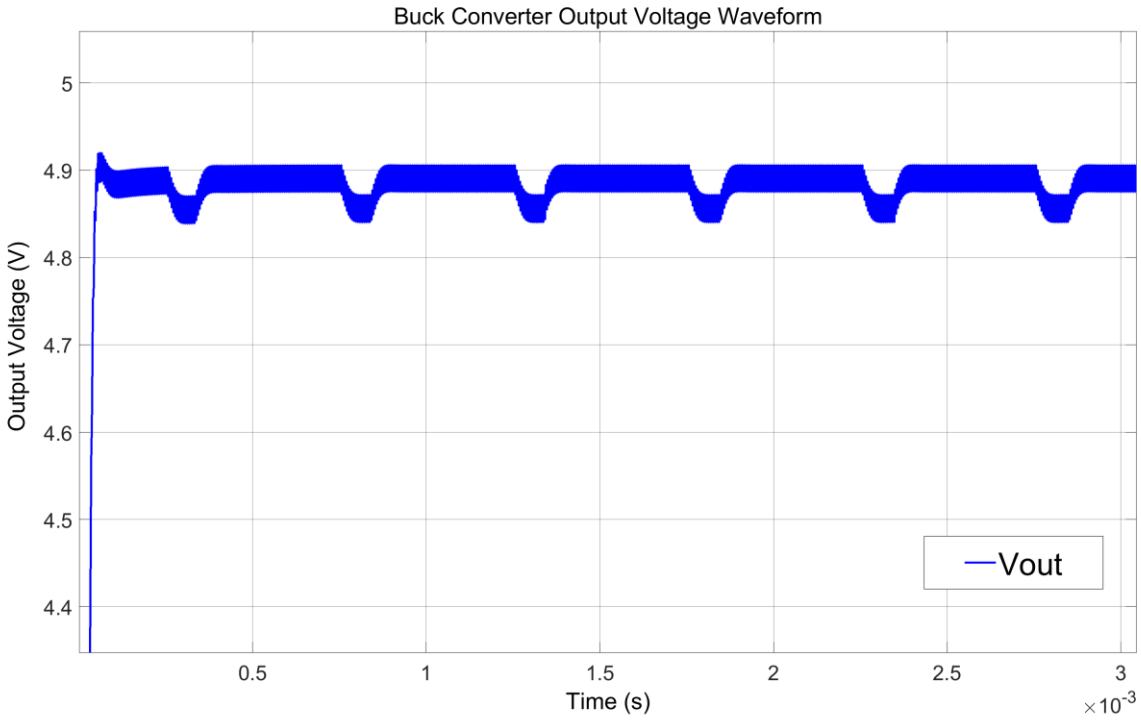

Figure 3-4. ZVS resonant buck converter output voltage simulation results Cr varied by adding and removing C2

Figure 3-4 shows the voltage output across the load resistor of the model in Figure 3-2. The slight dips in the output voltage are due to the increase in resonant capacitance when C2 is added to the C1 resonant capacitance. The C2 capacitor extends the ending of the MOSFET switching cycle, moving further down the resonance curve to decrease the output voltage, which using quasi-resonant switching reduces radiated noise.

3.2 PLL Feedback Control Design

3.2.1 Fixed Frequency Oscillator

A 555 timer chip circuit was used to create the fixed frequency oscillator (FFO) a simple implementation for setting the switching frequency for M1. The FFO circuit is shown in Figure 3-5.

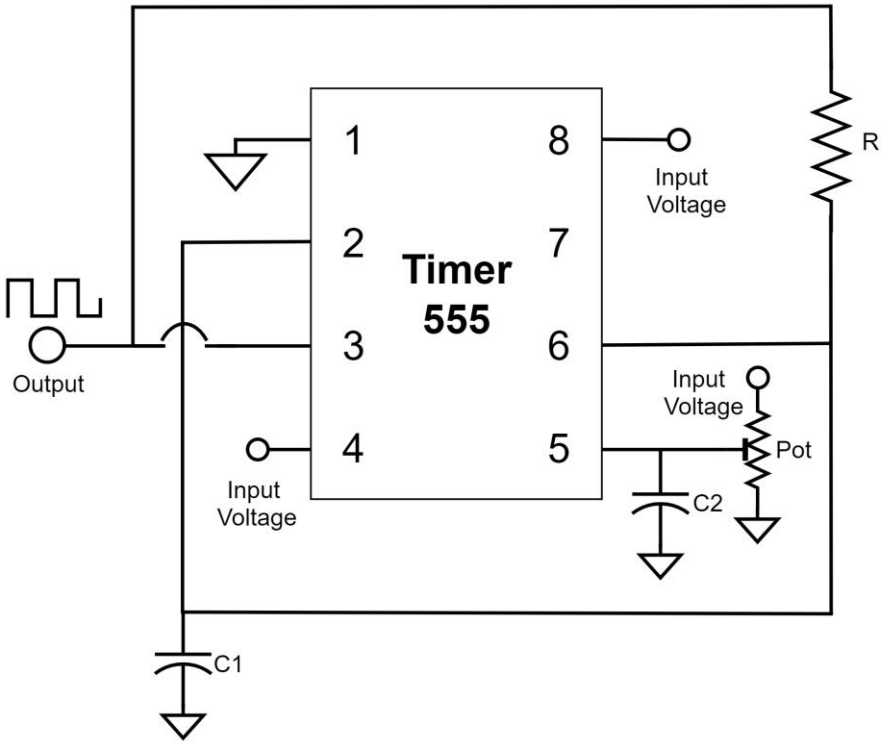

Figure 3-5. FFO circuit diagram [Christine Page]

In Figure 3-5, the capacitor C1 and resistor R form a RC network sat pin 2 to determine the output operating frequency. The potentiometer at pin 5 is used to control the duty cycle of the FFO between 10%-90%. Capacitor C2 filters the input voltage noise to reduce its affect on the output of the fixed frequency oscillator.

Equation (3.4) shows how to obtain the operation frequency of the FFO.

$$f = \frac{1}{1.1 * R * C1} \tag{3.4}$$

Table 3-2 shows the component values for the FFO.

Table 3-2. Table of Values for FFO

Description	Value
Operating Frequency	200 kHz
R	33 kOhm
C1	0.1 nF
C2	100 nF

3.2.2 Phase Frequency Detector

A PFD chip was used to implement the phase frequency detection function. Fig 3-6 shows the circuitry of the PFD chip [16].

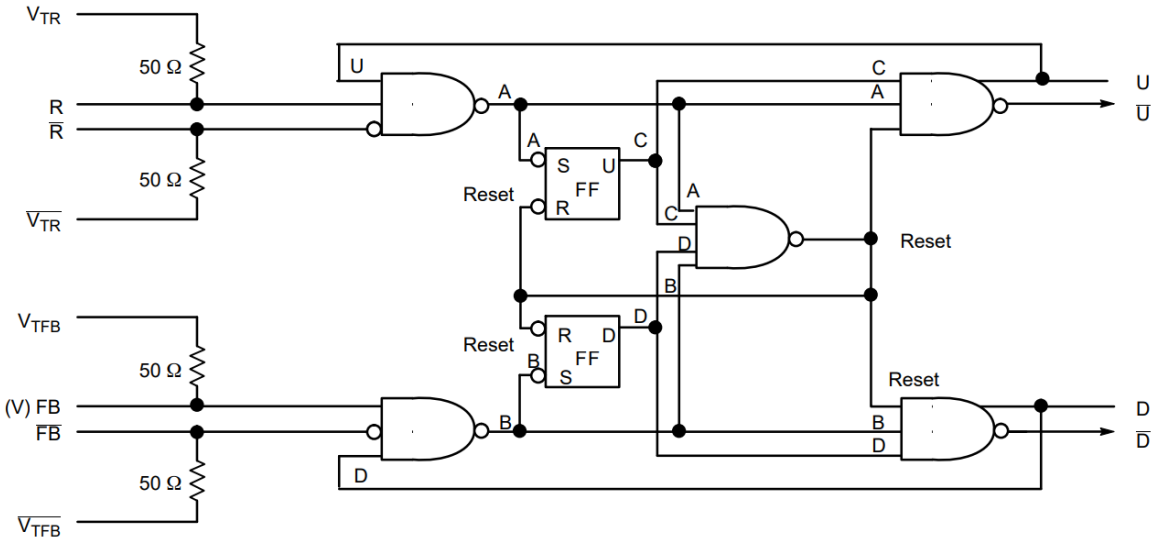

Figure 3-6. On Semiconductor's MC100EP40 PFD [16]

The PFD had four output paths: non-inverting UP output (U), inverting UP output ($\overline{U}$), non-inverting DOWN output (D), and inverting DOWN output ($\overline{D}$). Only the inverting UP output and non-inverting DOWN output are used for the controls in this design. The two input signals used are the feedback input (FB) and the reference input (R).

The reference input gets its voltage input from the VREF VCO referenced in Figure 3-2. The feedback input gets its voltage input from the overall output of the resonant buck

converter. When the reference for the resonant frequency observed on the output does not match the feedback input frequency, then the PFD will fix the frequency to match the feedback input frequency and the inverted UP signal will then connect to a high frequency charge pump chip to amplify the signal to switch a small signal MOSFET (M2).

3.2.3 Charge Pump

A charge pump chip was used to implement the charge pump. Figure 3-7 shows the circuitry of the charge pump chip [17].

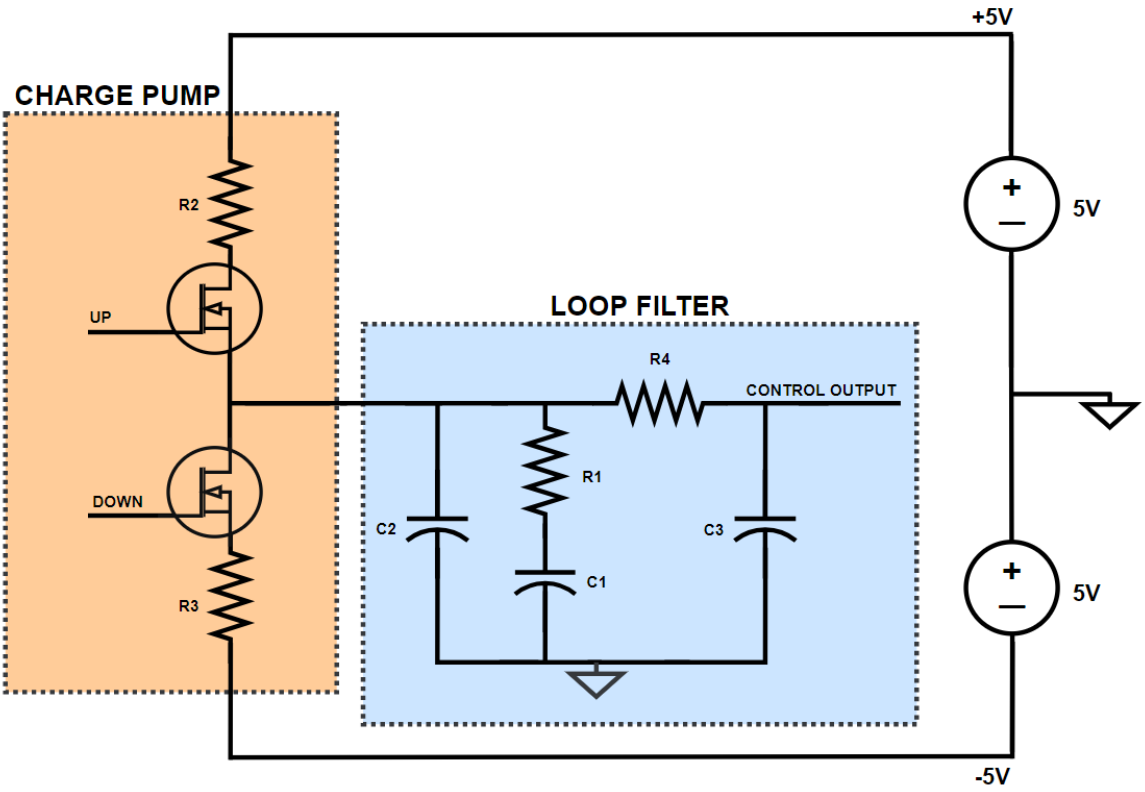

Figure 3-7. Charge Pump Chip Internal Circuit [17]

The charge pump takes the UP and DOWN signals generated from the PFD chip discussed in Section 3.3.2. The charge pump takes the logic states of the PFD and converts them into analog signals for control purposes.

The circuitry in orange in Figure 3-7 shows the charge pump, where the circuit discharges the current based on the value of the error of the UP and DOWN signal, which is calculated by the PFD. In Fig 3-7, the charging current is represented with voltage source +5 V connected to resistor R2, and the discharging current is represented with voltage source -5 V connected to resistor R3. The chip has a control input that can be set to a VREF. The ideal output of the resonant converter is 5 V, so the VREF of the charge pump was set to 5 V.

The circuitry in blue in Fig 3-7 shows the loop filter that is attached to the charge pump. The loop filter is preset within the chip to operate at a max frequency of 100 kHz. The control output in Figure 3-8 [17] connects to MOSFET M2 in Figure 3-2 to vary Cr depending on the state of M2.

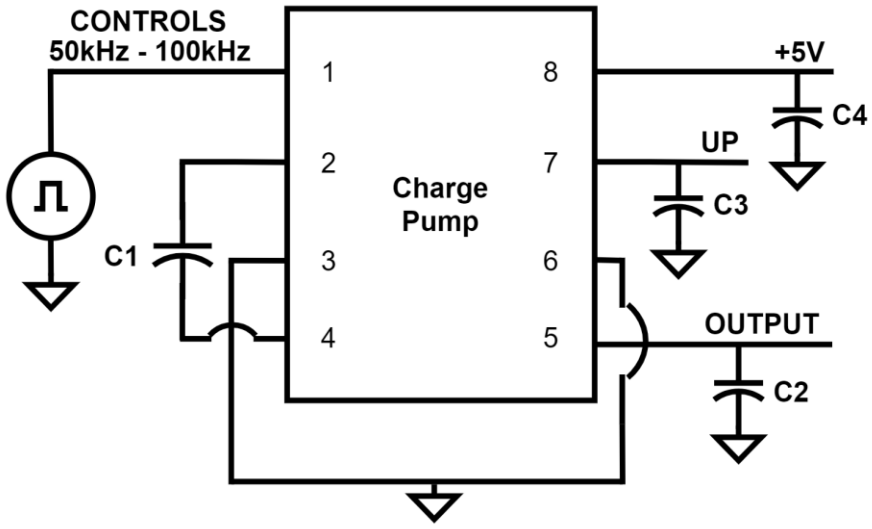

Figure 3-8. Charge Pump SP661 Chip Design [17]

Capacitors C1, C2, C3, and C4 in the SP661 datasheet diagram in Figure 3-8 are filter capacitors which are set to 33 uF due to the high frequency control inputs. The frequency applied to control the charge pump needs to be 50% of what the main switching frequency of MOSFET M1. The resonant converter is tested at both 200 kHz and 100 kHz switching frequencies. Therefore, to meet the switching requirement of the charge pump, it was operated

at 100 kHz when the converter was switching at 200 kHz and operated at 50 kHz when the converter was switching at 100 kHz.

3.2.4 Discrete Variable Capacitor

Figure 3-9 shows the feedback control for the resonant converter.

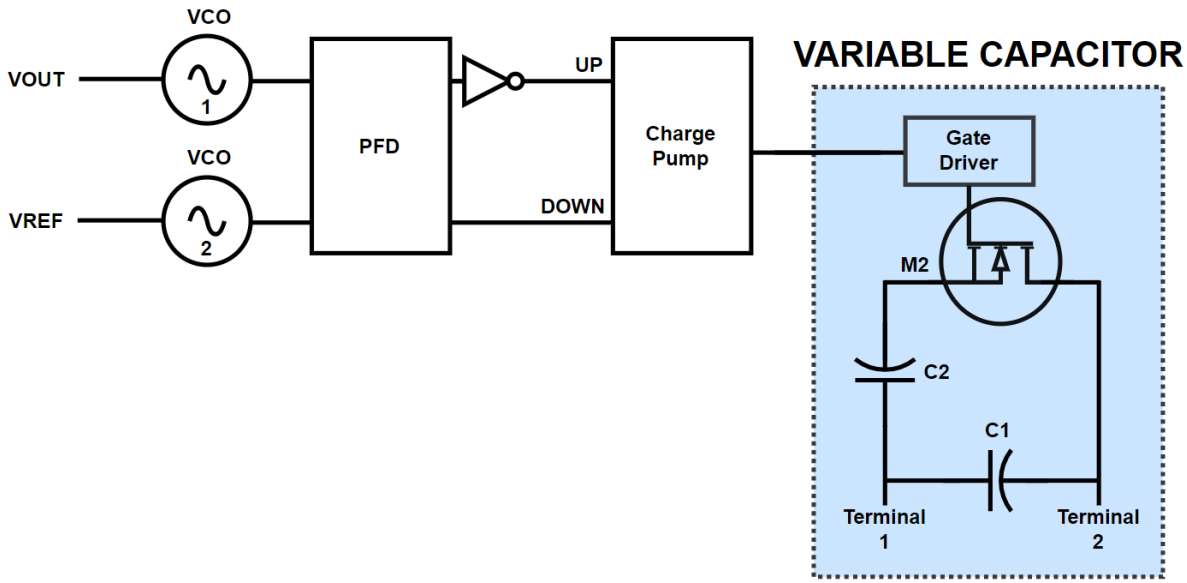

Figure 3-9. Resonant Converter Feedback Variable Capacitor Control [Christine Page]

The figure highlights that the varactor from [14] in blue that is implemented with a second capacitor, C2, switched in and out by a MOSFET M2 to connect C2 in parallel with the main resonant capacitor C1 when Cr needs to vary. Terminal 1 and Terminal 2 attach to drain and source, respectively, on MOSFET M1 of the power converter shown in Figure 3-2.

3.3 PCB Design for the Implemented Prototype

Figure 3-10 and Figure 3-11 shows the final PCB design and soldered board of the ZVS Resonant Buck Converter.

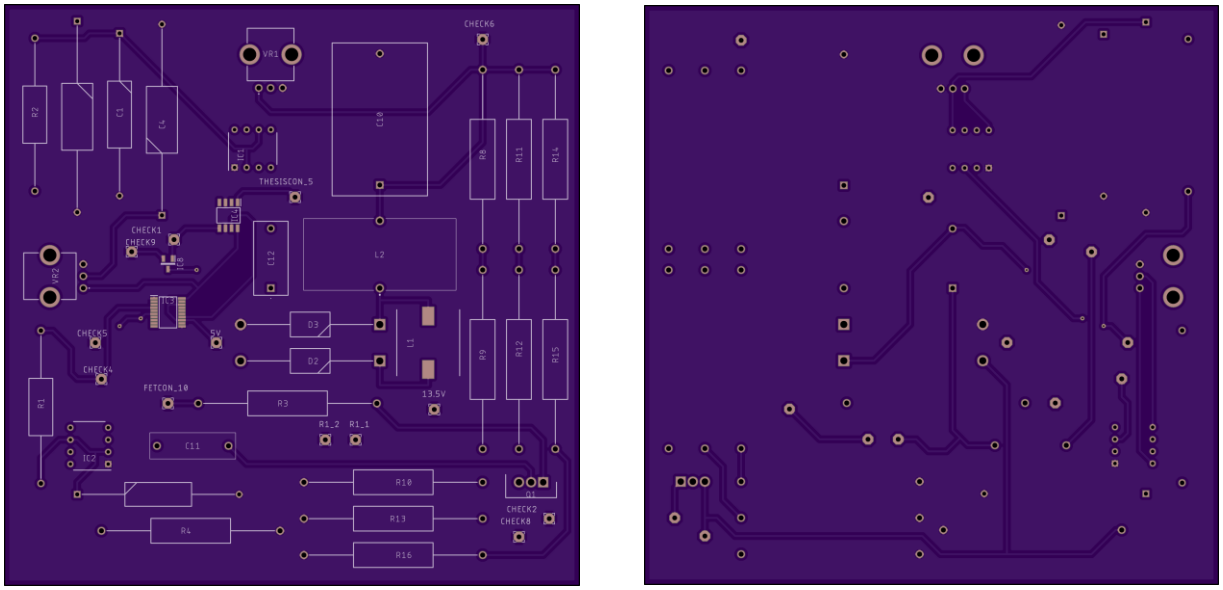

(a) Front Side **(b) Back Side**

Figure 3-10. Final PCB design of ZVS resonant buck converter [Christine Page]

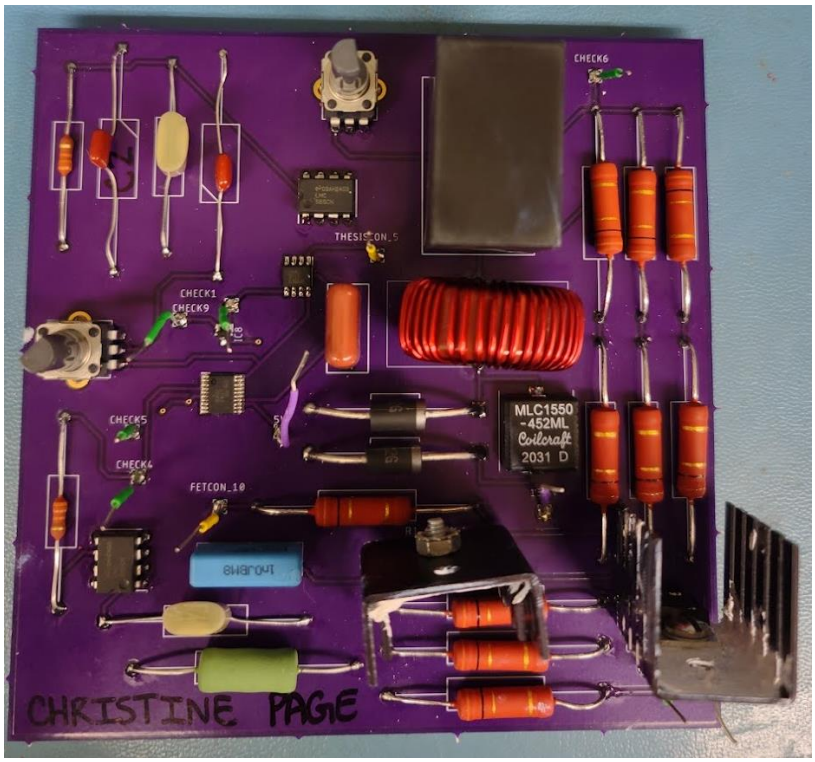

Figure 3-11. Final soldered ZVS resonant buck converter board 12cm x 12cm [Christine Page]

The dimensions of the board in Figure 3-11 are 12 cm by 12 cm. All components used are rated for low noise outputs in high frequency operations. To mitigate the noise due to long traces, all components are placed closely together. A resistor bridge is used for the load, instead of a single resistor, to be able to handle the high wattage output using a small resistance value, which is shown in Figure 3-12.

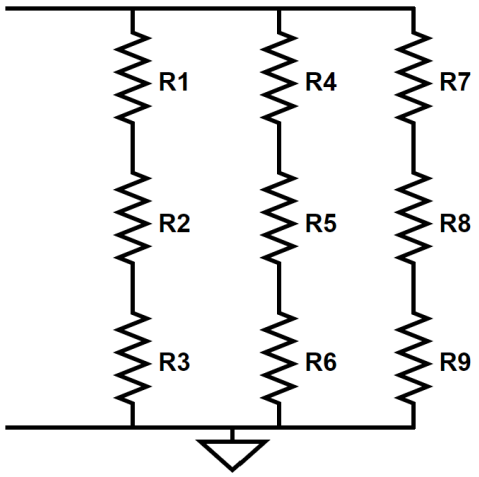

Figure 3-12. Resistor Bridge Load

The resistor bridge is a matrix of nine resistors, each of equal value, and has an overall equivalent resistance of 1.6 ohms as listed in Table 3-1.

A source-follower gate drive is designed to drive the MOSFET M1. The configuration is shown in Figure 3-13.

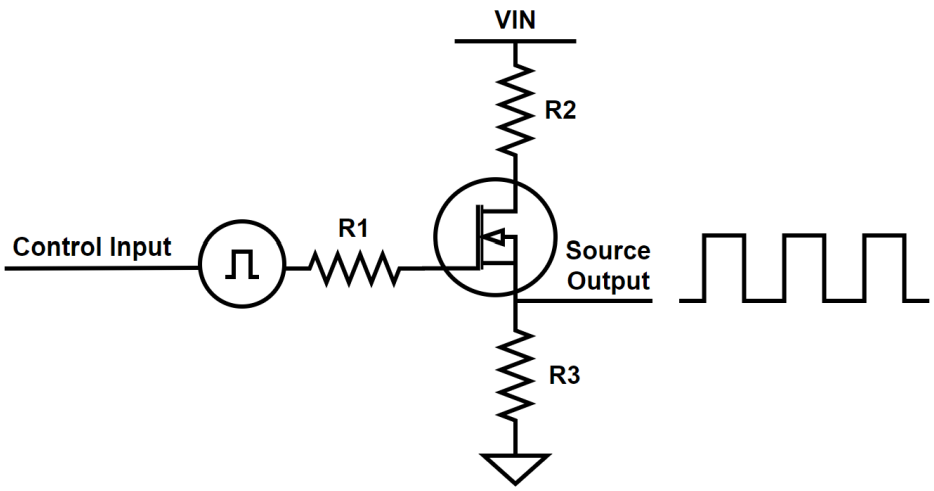

Figure 3-13. Source-Follower Gate Drive for MOSFET

3.4 Chapter Summary

A resonant buck converter incorporates both PWM and resonance schemes that reduce the noise of the overall system. A PLL control scheme is implemented with the main power MOSFET switching at a fixed frequency where a variable capacitor is used to vary the output voltage at the edge of the resonant curve to reduce the radiated noise output on the converter. The PLL control scheme takes a fixed reference voltage and the output converter voltage and the PFD and charge pump to control the MOSFET in series with a second capacitor to create a variable resonance capacitance for the resonant buck converter.

4.0 EXPERIMENTAL RESULTS

4.1 Testing Plan

Figure 4-1 shows the ZVS resonant buck converter design with Table 3-1 values included in the circuit. Figure 4-1 also shows the spectrum analyzer test points in blue.

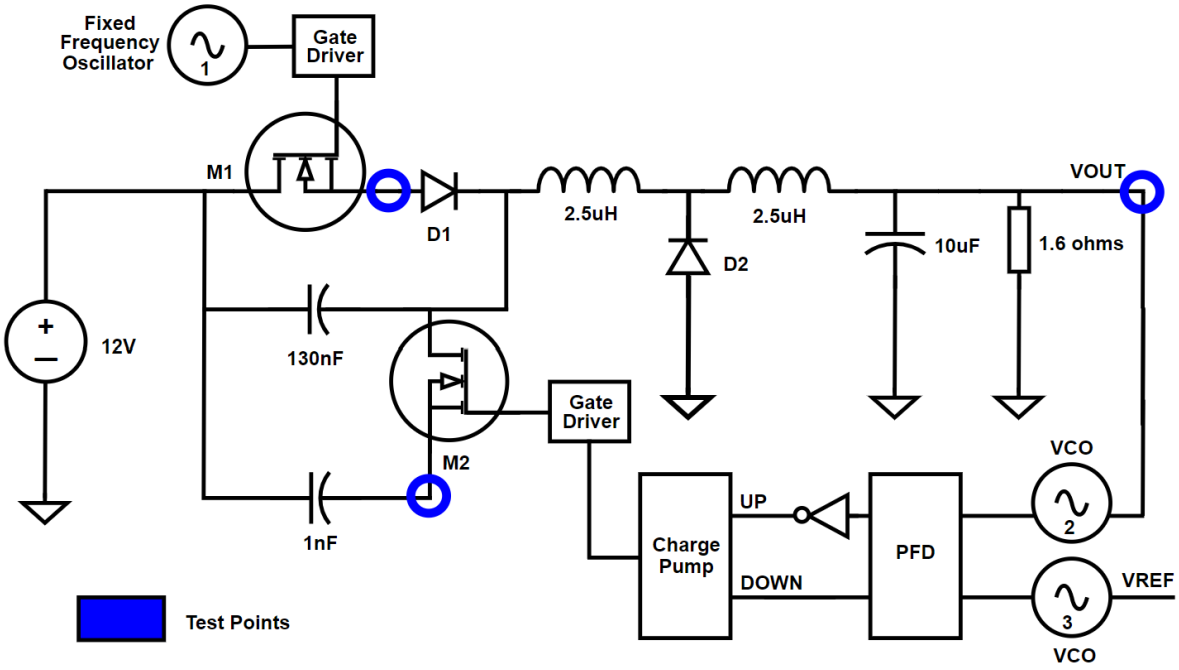

Figure 4-1. ZVS Resonant Buck Converter Design w/ Component Values & Test Points [Christine Page]

The resonant converter designed in Ch. 3 is compared to the basic buck converter with noise dampening techniques from Ch. 2. Figure 4-2 shows the basic buck converter design with components values included in the circuit. Figure 4-2 also shows the spectrum analyzer test points in blue.

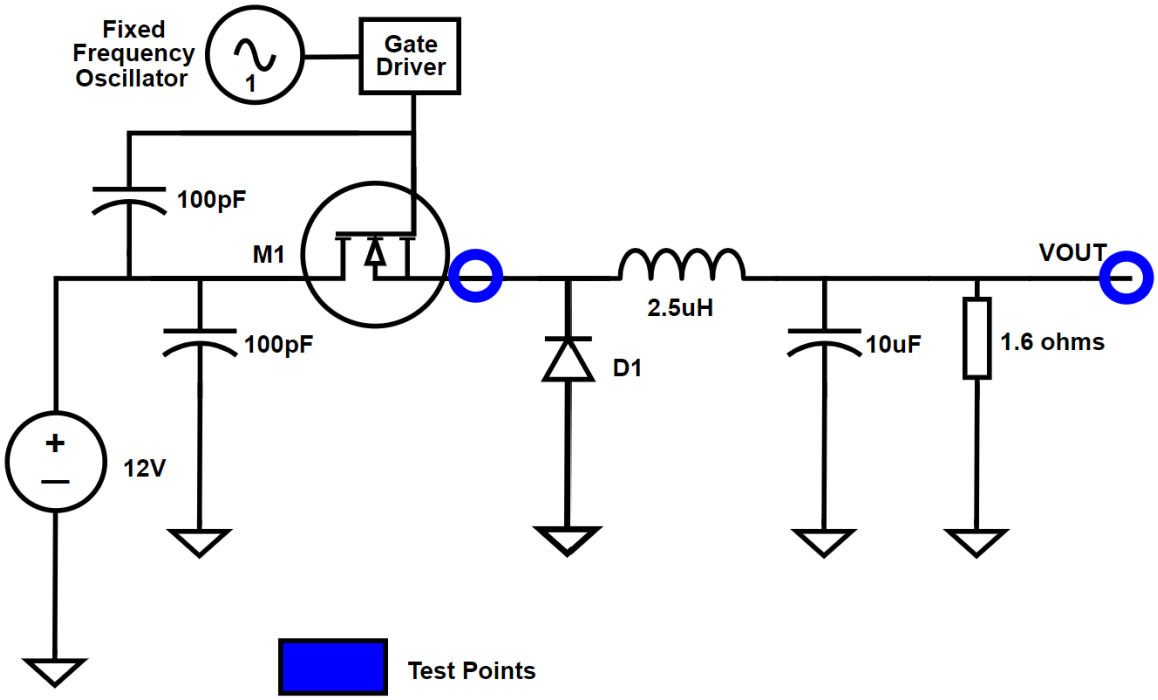

Figure 4-2. Basic Buck Converter Design w/ Component Values & Test Points [Christine Page]

A spectrum analyzer and RF probes are used to measure the noise in section 4.3.

Figure 4-3 shows the H-field RF probes used.

Figure 4-3. H-Field RF Probes

The probe with the circular loop end is used to narrow down where the most EMI is being emitted on the PC board. The probe is held so that the loop is perpendicular to the board and follows the current paths (traces) of the board. The oscilloscope is observed to see the RF noise level.

Once the area of EMI emission is identified, then the probe with the straight end will be used to identify and record which node is causing the RF noise output.

4.2 Resonant Converter Output Waveforms

Figure 4-4 shows experimental results of the ZVS resonant buck converter with the MOSFET switching at 200 kHz and the capacitor controls switching at 100 kHz.

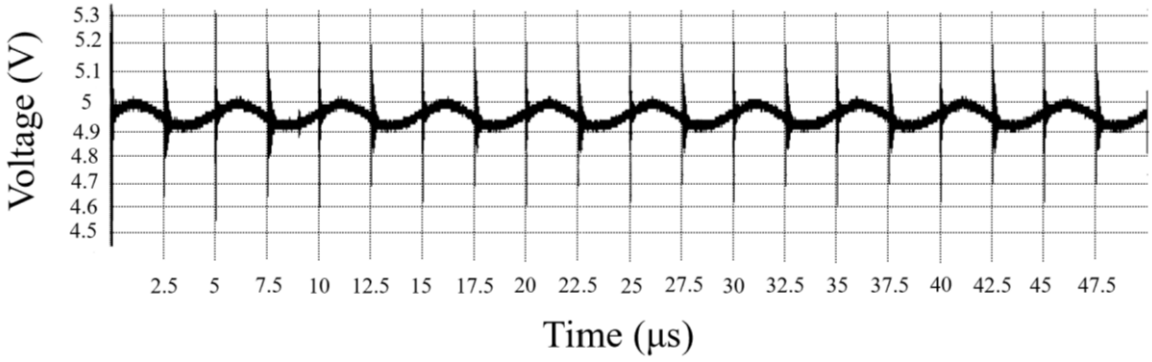

Figure 4-4. Output Voltage Waveform of Converter Switching at 200 kHz

The output voltage clearly changes from around 5 V to roughly 4.9 V. The 5 V output is when only the C1 capacitor is connected. The 4.9 V output is when C2 and C1 are combined in parallel. Figure 4-4 also shows that there is essentially no high frequency noise in the resonant switching, but there is still significant ringing due to hard switching of M2 which needs filtering.

Figure 4-5 shows results of the resonant buck converter with the MOSFET switching at 100 kHz and the controls switching at 50 kHz.

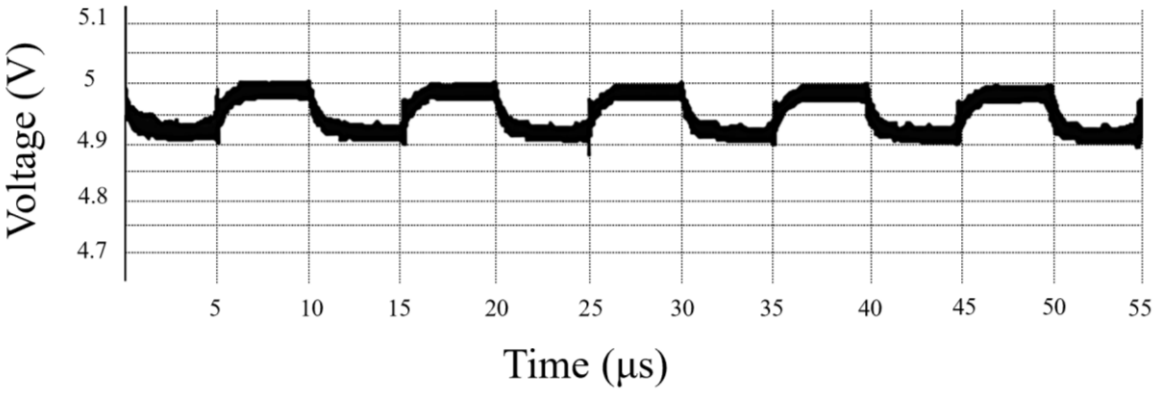

Figure 4-5. Output Voltage Waveform of Converter Switching at 100 kHz

The output voltage clearly changes from around 5 V to roughly 4.9 V. The 5 V output is when only the C1 capacitor is connected. The 4.9V output is when C2 and C1 are combined. At 100 kHz switching frequency for the resonant buck converter and 50 kHz for the controls, the output waveform levels out more distinctly at each level and more clearly show that the C2 capacitor does change the output voltage on the converter.

Figure 4-5 also shows again that there is no significant noise in the resonant switching while there is some ringing is due to the switching of M2 when adding in C2, but less than seen in Figure 4-4.

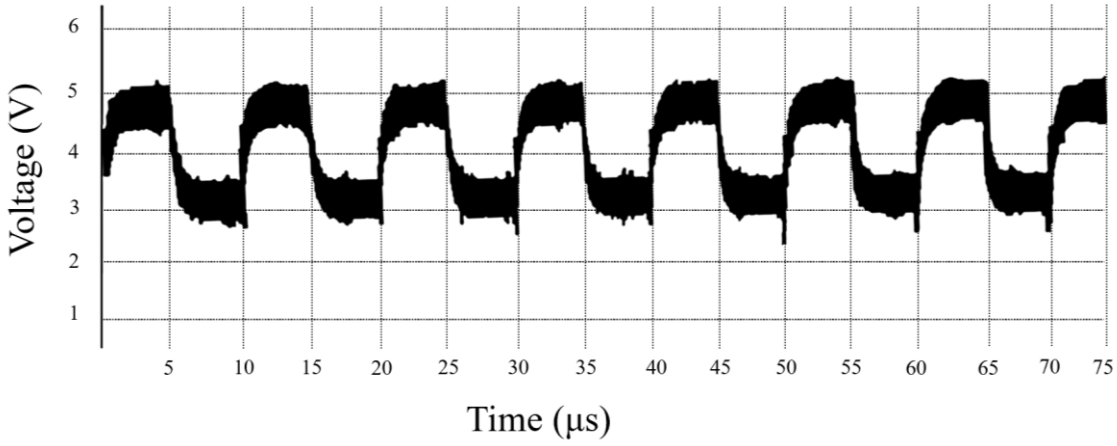

Figure 4-6. Output Voltage Waveform of Converter Switching at 100kHz with C2 = X uF

Figure 4-6 shows the results of the resonant buck converter with C2 increased to match the value of C1 which is 130 nF.

The output voltage clearly ranges from around 5 V to roughly 3 V. The 5 V output is when only the C1 capacitor is connected. The 3V output is when C2 and C1 are combined. The figure demonstrates that the range of variation of the output voltage can be increased by increasing the C2 capacitor value.

Figure 4-6 also shows that there is still no noise in the resonant switching, but significant ringing due to hard switching of M2. Even with the larger capacitance for C2, the resonant switching does not produce noise. This proves that the control scheme and converter enable voltage regulation at low noise.

4.3 Spectrum Analyzer Results

Figure 4-7 shows the spectrum analyzer results of a 200 kHz switching basic buck converter output.

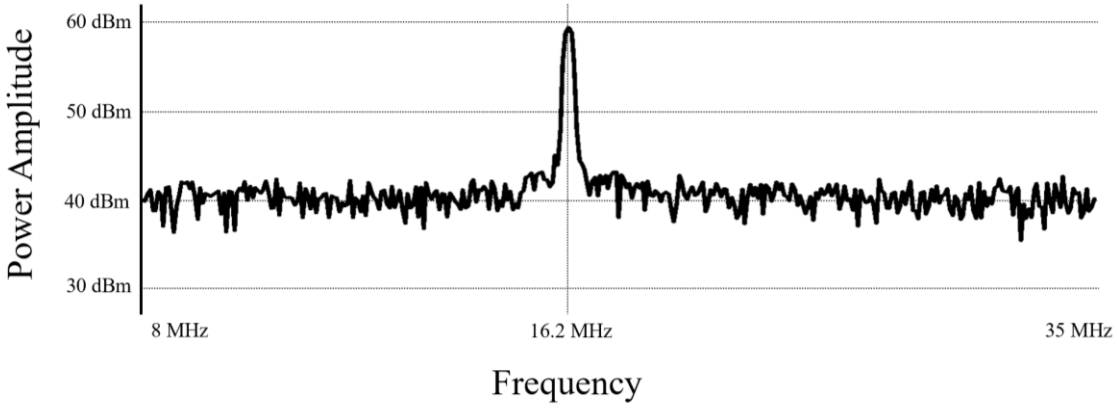

Figure 4-7. Spectrum Analyzer Results of 200 kHz Switching Basic Buck Converter Output

Figure 4-8 shows the spectrum analyzer results of the 200kHz switching resonant buck converter output.

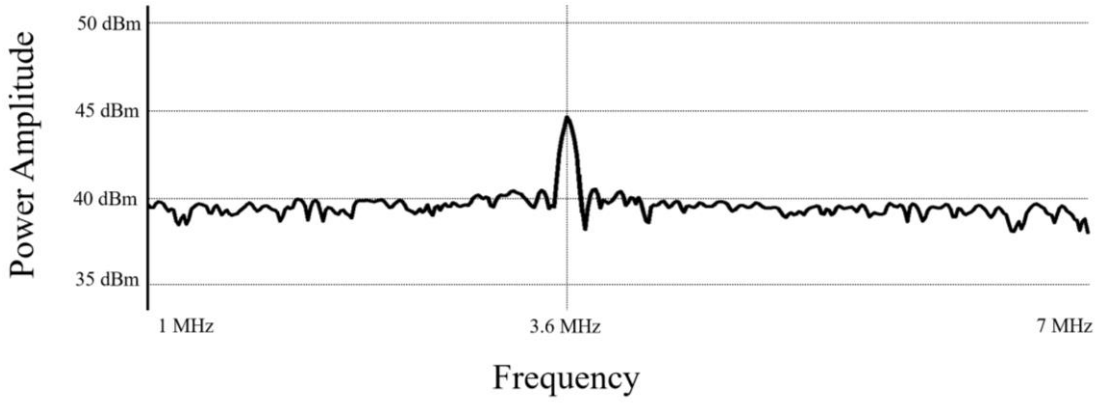

Figure 4-8. Spectrum Analyzer Results of 200 kHz Switching Resonant Buck Converter Output

The frequency amplitudes indicated in Figure 4-7 and Figure 4-8 are the largest amplitude and lowest frequency noise components directly created by switching. Figure 4-7 shows that the basic buck converter has a dominant component of noise around 16.2 MHz. The spike has an amplitude of around 60 dBm. Figure 4-8 shows the quasi-resonant buck converter has a noise amplitude peak at around 3.6 MHz. The switching noise peak is due to hard-switching of M2. The amplitude of spike is roughly 45 dBm. The spike is small and close to the noise floor. The resonant converter with a variable capacitor has a noise spike improvement of about 15 dBm when compared to the basic hard-switching buck converter as shown in Figure 4-7 and Figure 4-8.

Figure 4-9 shows the spectrum analyzer results between measurements at the basic buck converter MOSFET in orange and the resonant buck converter MOSFET in blue with both switching at 200 kHz.

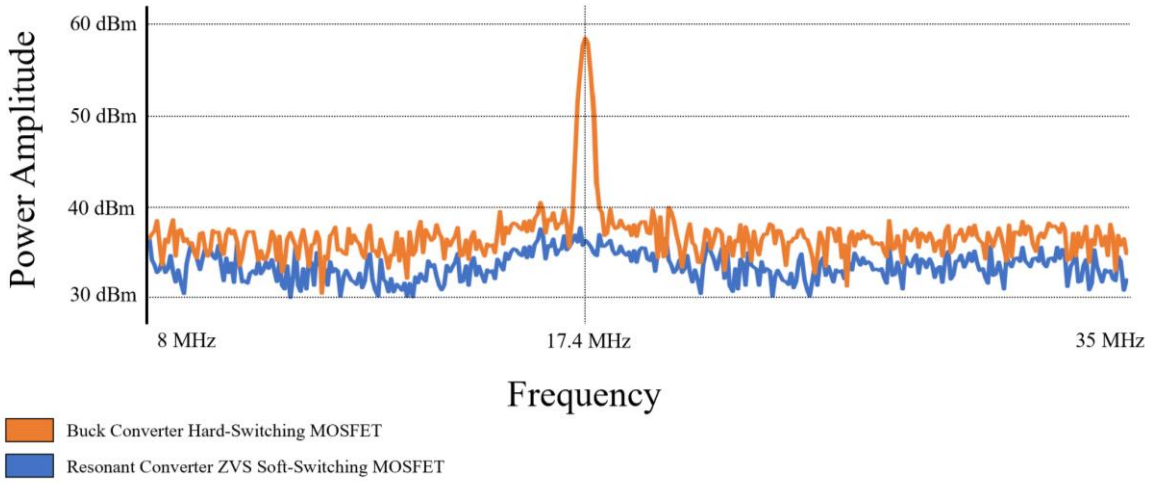

Figure 4-9. Spectrum Analyzer Results of 200 kHz Switching Basic Buck Converter MOSFET vs. 200 kHz Resonant Buck Converter MOSFET

Figure 4-9 clearly shows how the soft-switching resonant converter (blue) has eliminated most of the switching noise at the MOSFET terminal compared to the hard-switching buck converter (orange). There is no longer a noise spike at 17.4 MHz when measuring the resonant converter. The different noise spike measurements are due to the RF probes used. There are also no noise spikes of significance within the same range of frequencies.

Figure 4-10 shows the spectrum analyzer results for the resonant converter variable capacitor (C2) MOSFET (M2).

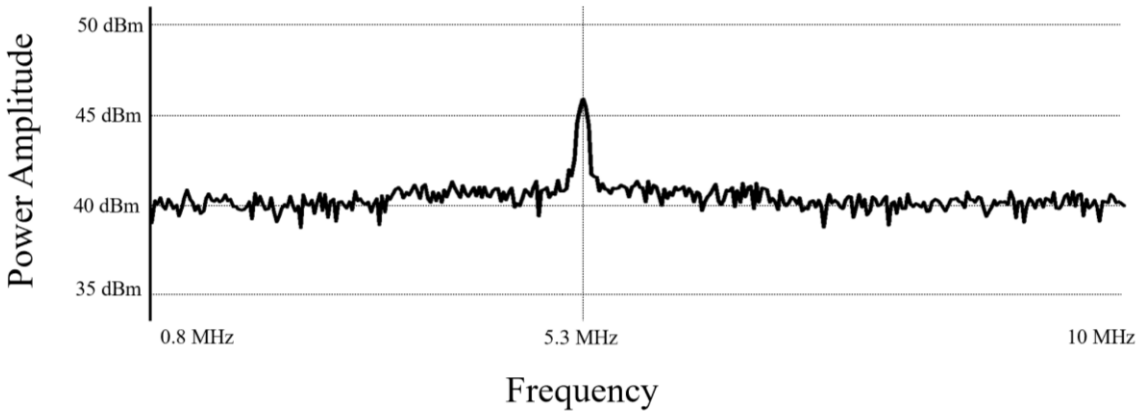

Figure 4-10. Spectrum Analyzer Results for Variable Capacitor MOSFET

The MOSFET switching the variable capacitor in and out is using hard-switching, which is where the noise spike at 5.3 MHz is originating from.

4.4 Chapter Summary

The ZVS resonant converter with a variable capacitor has a noise improvement of about 80% when compared to the basic hard-switching buck converter. The results prove that the ZVS resonant converter switching with a variable capacitor is a superior alternative to the buck converter when wanting to reduce the output noise of a power converter.

5.0 CONCLUSIONS

For the CubeSat power supply presented in this work, a quasi-resonant ZVS converter has been designed and tested to replace the standard buck. The resonant converter design enables a further reduction in power converter volume and weight. This thesis is a culmination of work designing and integrating a PLL control scheme to create a variable capacitance to vary the voltage output on a soft-switching quasi-resonant buck converter to reduce the RF noise output of the converter due to the MOSFET switching.

In the innovative resonant power converter control strategy proposed in this thesis, the roles of PWM signal and resonant filter are reversed: in the resonant power converter, the oscillator controlling the power MOSFET is at a fixed frequency and the resonant circuit has a variable capacitance that enables the control of the resonance frequency to control the output voltage. The design of the resonant control was presented and discussed in Chapter 3.

Control signals for a power supply in a CubeSat are susceptible to noise that is coupled through voltage. By converting the information in control signals from voltage to frequency, switching noise is not coupled into the feedback and error signals. The research functions of the CubeSat are also susceptible to the switching noise. The results presented in Chapter 4 demonstrate that the ZVS resonant converter switching in a variable capacitor is a superior alternative to the buck converter for reducing the output noise from a power converter. The resonant converter with a variable capacitor has a noise spike improvement of about 15 dBm when compared to the basic hard-switching buck converter discussed in Chapter 2 as demonstrated in Chapter 5.

6.0 FUTURE WORK

The 100 kHz bandwidth limitation of the PLL control scheme connected to the variable capacitor is the biggest problem with the design of the fixed frequency ZVS quasi-resonant converter presented in this thesis. Another limitation is the inability to operate the varying capacitance values without the help of an integrated switching procedure which produces unnecessary noise, albeit small, on the output of the converter. Research should be continued on the development of a wider-bandwidth control scheme for even higher frequency operations as well as the design of a varactor diode to act as the variable capacitor instead of the series MOSFET and capacitance scheme shown in this thesis.

6.1 Design of a Resonant Converter with a Varactor Diode for Variable Capacitance

A varactor diode is able to act as a variable capacitor. A varactor's capacitance value varies electrically based on the applied reverse voltage. The structure of the varactor diode is shown in Figure 6-1 [18].

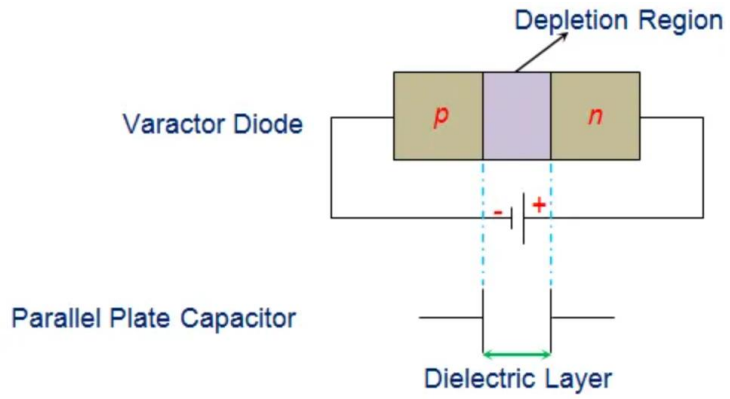

Figure 6-1. Varactor Diode Operation Breakdown [18]

The depletion region is labeled as the dielectric layer. The dielectric layer expands when the voltage applied increases, resulting in the P-N layers being further separated. This

causes the capacitance value to decrease. When the dielectric layer shrinks as the applied voltage applied decreases, the P-N layers is closer together. This causes the capacitance value to increase.

Figure 6-2 shows a modified control scheme with a varactor diode.

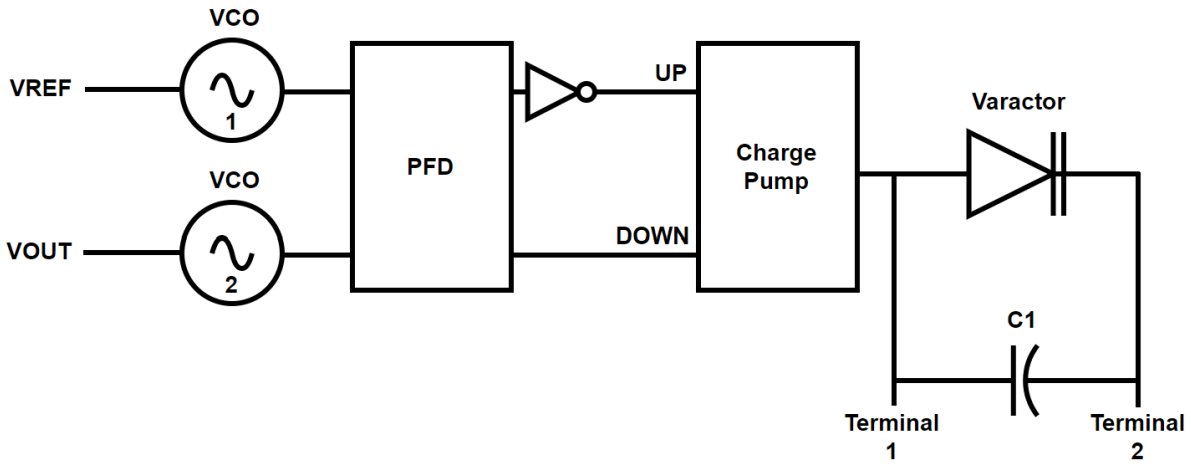

Figure 6-2. Varactor Controls [Christine Page]

Figure 6-2 shows the varactor diode replacing the capacitor C2 and the associated MOSFET, M2. Instead of having a MOSFET hard-switching to add and remove the capacitor C2 to vary the effective resonant capacitance, Cr, the varactor can vary its effective capacitance based on the inverse voltage from the output of the control scheme (through the output of the charge pump). Using a varactor also eliminates the need to physically replace C2 with a different capacitor to change the voltage output since varying the reverse voltage on the varactor will then vary the effective capacitance value over a continuous range.

Equation (6.1) describes the capacitance value of the varactor diode.

$$C_j = \frac{\varepsilon * A}{d} \tag{6.1}$$

where, C_j is the total capacitance of the junction, ε is the permittivity of the semiconductor material, A is the cross-sectional area of the junction, and d is the width of the depletion region.

Equation (6.2) describes the effective capacitance value of the varactor diode using the reverse bias voltage and capacitor of the varactor diode when unbiased.

$$C_j = \frac{C*K}{(V_b - V_R)^m} \tag{6.2}$$

where, C is the effective capacitance of the varactor diode when unbiased, K is the constant (normally is considered to be 1) [18], V_b is the barrier potential, V_R is the applied reverse voltage, and m is a material-dependent constant.

Figure 6-3 shows the electrical equivalent circuit of the varactor diode.

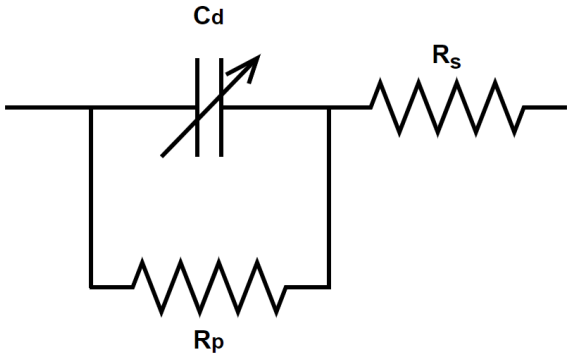

Figure 6-3. Varactor Diode Equivalent Circuit

Equation (6.3) can be used to calculate the maximum operating frequency of the varactor.

$$F = \frac{1}{2*\pi*R_s*C_j} \tag{6.3}$$

6.2 VCO with Varactor Diode

The thesis covers the design and testing of a 200 kHz fixed frequency resonant converter for a CubeSat. However, Table 2-1 indicates that a CubeSats switching frequency

needs to be able to have a range with the minimum frequency of 100 kHz, the mid-range frequency of 150 kHz, and the maximum frequency of 200 kHz. The implemented control scheme reduces noise with a fixed frequency switching scheme and varying the duty cycle on the VCOs created by the 555 timers as discussed in Section 3.2.1. To be able to change the fixed frequency reference, a varactor diode also needs to be implemented in the VCOs.

Figure 6-4 shows a VCO circuit configuration with a varactor implemented in its design.

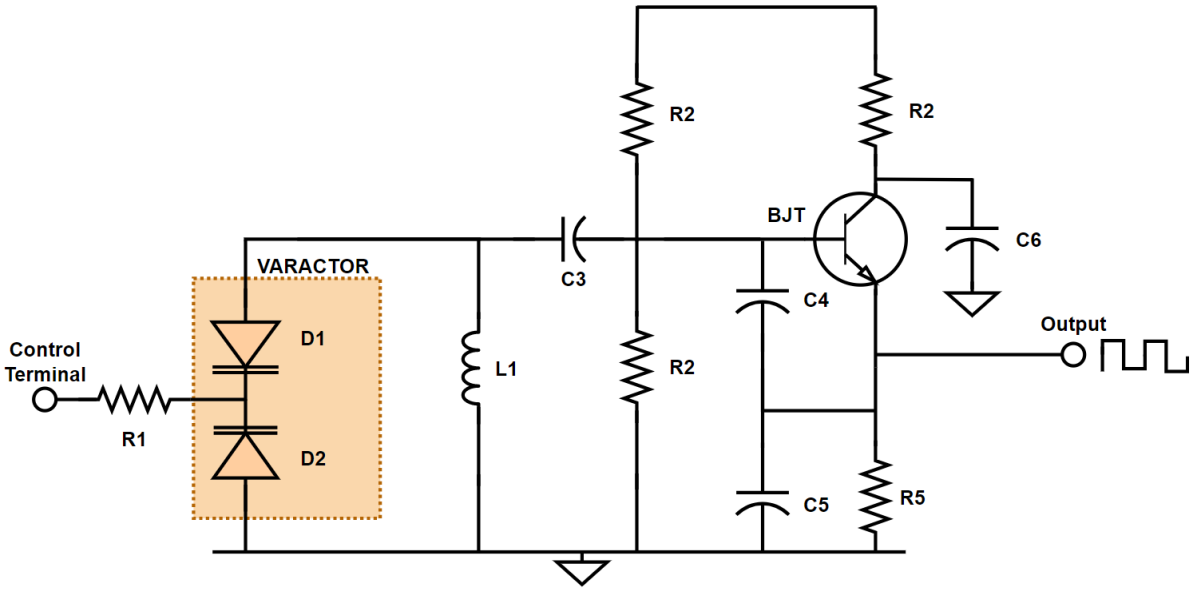

Figure 6-4. VCO w/ Varactor Diode [Christine Page]

6.3 Pulse Density Modulation Control Scheme Integration

Pulse density modulation (PDM) is a form of modulation to represent an analog signal with a binary signal [19]. If the voltage is too low on the first switching cycle, the next switching cycle will be set to a higher output voltage level. If the output is too low, the next switching cycle will be at a lower voltage level. The desired voltage level will be between the two levels, and the varactor should be able to vary its effective capacitance value appropriately to provide the desired resonant converter output voltage.

6.4 Chapter Summary

For the future work, the resonant converter control scheme needs to have the ability to vary the effective C2 capacitance value. To be able to compensate for the output voltage at high frequencies, a pulse density modulation control scheme can be implemented into the presented control scheme in this thesis. The PDM control scheme is needed in order to be able to provide the best variety of voltage values

REFERENCES

[1] National Aeronautics and Space Administration (NASA) (2018). *NASA Strategic Plan 2018.* https://www.nasa.gov/sites/default/files/atoms/files/nasa_2018_strategic_plan.pdf

[2] National Aeronautics and Space Administration (NASA) (2020). *2020 NASA Technology Taxonomy*. https://www.nasa.gov/sites/default/files/atoms/files/2020_nasa_technology_taxonomy_lowres.pdf

[3] National Aeronautics and Space Administration (NASA). *DC/DC Converter Lesson Learned*. https://llis.nasa.gov/lesson/1879

[4] National Aeronautics and Space Administration (NASA*). Tally of problems and failures encountered for DC/DC Converters used in space programs*. https://nepp.nasa.gov/dcdc/failurelog.htm

[5] Brown, S. (2019, June 24). *Difference between noise and signal.* http://www.differencebetween.net/science/difference-between-noise-and-signal/#:~:text=A%20signal%20is%20also%20an%20original%20sound%20while,signal%20to%20noise%20ratio%20of%20noise%20is%20low.

[6] Committee on a Survey of the Active Sensing Uses of the Radio Spectrum. (2015). *A strategy for active remote sensing amid increased demand for radio spectrum.* National Academies Press.

[7] *EN 55011 CISPR* 11. (n.d.). Celectronics. https://celectronics.com/training/learning/method/EN55011.html

[8] In Compliance Magazine. 2021. *Radiated EMI From A Buck Converter - In Compliance Magazine.* https://incompliancemag.com/article/radiated-emi-from-a-buck-converter.

[9] Texas Instruments. (2020, August). *TPS6291x 3-V to 17-V, 2-A/3-A Low Noise and Low Ripple Buck Converter with Integrated Ferrite Bead Filter Compensation.* https://www.ti.com/lit/ds/symlink/tps62912.pdf?ts=1620917993828&ref_url=https%253A%252F%252Fwww.ti.com%252Fpower-management%252Fnon-isolated-dc-dc-switching-regulators%252Fstep-down-buck%252Fbuck-converter-integrated-switch%252Foverview.html.

[10] Hart, D. (2010). *Power Electronics* (1st ed.). McGraw Hill.

[11] Private communication with K. Cahoy, lecture notes from MIT 16.851 Satellite Engineering Fall 2020.

[12] AAC Clyde Space. (2022, March 14*). AAC Clyde Space | Small Satellite Spacecraft Providers*. https://www.aac-clyde.space/

[13] Zhaksvlvk, A. (2019). Implementation of a phase shifted full bridge DC-DC ZVS converter (September 2019). Universidad de Oviedo.

[14] Prabal Upadhyaya, M.S., "A Fully Integrated Buck Converter with Varactor Phase-Locking Control Scheme," December 2007.

[15] Wolf, S. (1983). *Guide to Electronic Measurements in Laboratory Practice*. Second Edition, Prentice-Hall.

[16] onsemi. (n.d.). MC100EP40: Phase-Frequency Detector, 3.3 V / 5 V, ECL Differential. https://www.onsemi.com/products/timing-logic-memory/clock-generation/phase-frequency-detectors/mc100ep40

[17] S.P.C. (n.d.). SP6661 Datasheet(PDF) - Sipex Corporation. All Data Sheet. https://www.alldatasheet.com/datasheet-pdf/pdf/80721/SIPEX/SP6661.html

[18] P. (2021, May 3). *Varactor Diode*. ProtonsTalk. https://protonstalk.com/semiconductors/varactor-diode/

[19] Kassakian, J. G., Schlecht, M. F., & Verghese, G. C. (1991). *Principles of Power Electronics* (Facsimile ed.). Pearson College Div.